Overview of the Manitou Experimental Forest Observatory: Site description and selected science results from 2008-2013

J. Ortega[1], A. Turnipseed[1], A. B. Guenther[1,a], T. G. Karl[1,b], D. A. Day[2], D. Gochis[1], J. A. Huffman[3,4], A. J. Prenni[5], E. J. T. Levin[5], S. M. Kreidenweis[5], P. J. DeMott[5], Y. Tobo[5], E. G. Patton[1], A. Hodzic[1], Y. Y. Cui[6], P. C. Harley[1,c], R. S. Hornbrook[1], E. C. Apel[1], R. K. Monson[7], A. S. D. Eller[8,d], J. P. Greenberg[1], M. Barth[1], P. Campuzano-Jost[2], B. B. Palm[2], J. L. Jimenez[2], A. C. Aiken[9], M. K. Dubey[9], C. Geron[10], J. Offenberg[11], M. G. Ryan[12,13], P. J. Fornwalt[13], S. C. Pryor[14], F. N. Keutsch[15], J. P. DiGangi[15,e], A. W. H. Chan[16,f], A. H. Goldstein[16,17], G. M. Wolfe[18,19], S. Kim[1,g], L. Kaser[20,h], R. Schnitzhofer[20], A. Hansel[20], C. A. Cantrell[1,i], R. L. Mauldin[1,i], J. N. Smith[1]

[1]National Center for Atmospheric Research, P.O. Box 3000, Boulder, CO 80307, USA

[2]University of Colorado, Department of Chemistry and Biochemistry and CIRES, Boulder, CO 80309, USA

[3]Max Planck Institute for Chemistry, P.O. Box 3060, 55020, Mainz, Germany

[4]University of Denver, Department of Chemistry & Biochemistry, Denver, CO 80208, USA

[5]Department of Atmospheric Science, Colorado State University, Fort Collins, CO 80523, USA

[6]Department of Earth and Atmospheric Sciences, Saint Louis University, MO 63103, USA

[7]School of Natural Resources and the Environment and Laboratory for Tree Ring Research, University of Arizona, Tucson, Arizona 85721, USA

[8]Cooperative Institute for Research in Environmental Sciences (CIRES), University of Colorado, Boulder, CO 80309, USA

[9]Los Alamos National Laboratory, Earth and Environmental Sciences Division, Los Alamos, NM 87545, USA

[10]U.S. Environmental Protection Agency, Office of Research and Development, National Risk Management Research Laboratory, Air pollution Prevention and Control Division, Research Triangle Park, NC 27711, USA

[11]United States Environmental Protection Agency, Office of Research and Development, National Exposure Research Laboratory, Research Triangle Park, NC 27711, USA

[12]National Resource Ecology Laboratory, Colorado State University, Fort Collins, CO 80523, USA

[13]United States Department of Agriculture, Forest Service, Rocky Mountain Research Station, 240 West Prospect Rd., Fort Collins, CO 80526, USA

[14]Department of Geological Sciences, Indiana University, Bloomington IN 47405, USA

[15]Department of Chemistry, University of Wisconsin, Madison, WI 53706, USA

[16]Department of Environmental Science, Policy and Management, University of California, Berkeley, CA, 94720, USA

[17]Department of Civil and Environmental Engineering, University of California, Berkeley, CA, 94720, USA

[18]Atmospheric Chemistry and Dynamics Laboratory, Goddard Space Flight Center, 8800 Greenbelt Road, Greenbelt, MD 20771, USA

[19]Joint Center for Earth Systems Technology, University of Maryland Baltimore County, Baltimore County, MD 21250, USA

[20]Institute for Ion Physics and Applied Physics, University of Innsbruck, Innsbruck, Austria

Corresponding author: jimsmith@ucar.edu, (303) 497-1468

[a]Now at: Pacific Northwest National Laboratory, Atmospheric Sciences Division, P.O. Box 999 Richland, WA 99352, USA

[b]Now at: University of Innsbruck, Institute for Meteorology and Geophysics (IMGI), Innrain 52, 6020 Innsbruck, Austria

[c]Now at: Department of Plant Physiology, Estonian University of Life Sciences, Tartu 51014, Estonia

[d]Now at: Department of Biological Sciences, Macquarie University, Sydney, NSW, 2109, Austrailia

[e]Now at: NASA Langley Research Center, Chemistry and Dynamics Branch, Hampton, Virginia 23681, USA

[f]Now at: Now at Department of Chemical Engineering and Applied Chemistry, University of Toronto, Canada

[g]Now at Department of Earth System Science, University of California, Irvine, Irvine, CA 92697, USA

[h]Now at National Center for Atmospheric Research, P.O. Box 3000, Boulder, CO 80307, USA

[i]Now at Department of Atmospheric and Oceanic Sciences, University of Colorado, Boulder, CO 80309, USA

Modified draft based on reviewer comments; Atmospheric Chemistry and Physics: Manuscript number ACP-2013-685; April 29, 2014

Abstract

The Bio-hydro-atmosphere interactions of Energy, Aerosols, Carbon, H_2O, Organics & Nitrogen (BEACHON) project seeks to understand the feedbacks and inter-relationships between hydrology, biogenic emissions, carbon assimilation, aerosol properties, clouds and associated feedbacks within water-limited ecosystems. The Manitou Experimental Forest Observatory (MEFO) was established in 2008 by the National Center for Atmospheric Research to address many of the BEACHON research objectives, and it now provides a fixed field site with significant infrastructure. MEFO is a mountainous, semi-arid ponderosa pine-dominated forest site that is normally dominated by clean continental air, but is periodically influenced by anthropogenic sources from Colorado Front Range cities. This article summarizes the past and ongoing research activities at the site, and highlights some of the significant findings that have resulted from these measurements. These activities include:

- soil property measurements,
- hydrological studies,
- measurements of high-frequency turbulence parameters,
- eddy covariance flux measurements of water, energy, aerosols and carbon dioxide through the canopy,
- determination of biogenic and anthropogenic volatile organic compound emissions and their influence on regional atmospheric chemistry,
- aerosol number and mass distributions,
- chemical speciation of aerosol particles,
- characterization of ice and cloud condensation nuclei,
- trace gas measurements, and

- model simulations using coupled chemistry and meteorology.

In addition to various long-term continuous measurements, three focused measurement campaigns with state-of-the-art instrumentation have taken place since the site was established, and two of these studies are the subjects of this special issue: BEACHON-ROCS (Rocky Mountain Organic Carbon Study; 2010) and BEACHON-RoMBAS (Rocky Mountain Biogenic Aerosol Study; 2011).

1. Introduction

1.1 Motivation

Development of Earth-System models is driven by the need to improve the predictability of atmospheric chemical and physical processes over time scales ranging from minutes to decades. Accurate model predictions are contingent on process-level understanding and detailed numerical descriptions of the coupling between water, energy and biogeochemical cycles across temporal and spatial scales (Denman et al., 2007, Alo and Wang 2008, Heald et al., 2009). A number of studies have discussed some of these processes and associated feedbacks (e.g. Barth et al., 2005, Carslaw et al., 2010, Mahowald et al., 2011), but more detailed observations and coordinated modeling efforts are required for improved representation in Earth-System models.

The Bio-hydro-atmosphere interactions of Energy, Aerosols, Carbon, H_2O, Organics & Nitrogen (BEACHON) project was initiated by the National Center for Atmospheric Research (NCAR) as well as research collaborators from the university community to investigate ecosystem-atmosphere exchange of trace gases and aerosols and their potential feedbacks between biogeochemical and water cycles. BEACHON is now an ongoing component of atmospheric research sponsored by the National Science Foundation. This interdisciplinary research program integrates local and regional model simulations with remote sensing, regional network observations, and canopy- to regional-scale field measurements. BEACHON includes investigations of atmospheric, ecological and hydrological processes including concentration and flux measurements of energy, CO_2, H_2O, volatile organic compounds, aerosols, nitrogen compounds, hydrological parameters and feedback processes that are relevant to atmospheric chemistry. Rocky Mountain ecosystems are important for providing water and other resources in

the western United States, but contain only a limited number of long-term monitoring sites. This region is predominantly arid or semi-arid resulting in biogeochemical cycles that are water-limited. Since the area contains some of the fastest growing population centers, water limitations (combined with a climate that is projected to be warmer and potentially drier) pose significant societal vulnerabilities (Vorosmarty et al., 2010). The region's remote complex terrain leads to highly variable ecosystem characteristics, and it is unclear how this variability affects hydrological and atmospheric processes across larger geographical areas. The need for long-term land-ecosystem-atmosphere observation networks has been identified by international research programs as a key need for advancing Earth System science (Guenther et al., 2011).

To address these challenges, the BEACHON project in collaboration with the United States Department of Agriculture (USDA) Forest Service established the Manitou Experimental Forest Observatory (MEFO) in 2008, in an area representative of a middle-elevation (~2000 – 2500 m a.s.l.), semi-arid, ponderosa pine ecosystem that is common throughout the Rocky Mountain West, but not adequately characterized. The BEACHON project and establishment of this site were designed to meet the following objectives:

- Collect long-term measurements of meteorology, water, carbon dioxide (CO_2), and energy fluxes, aerosol size distributions and fluxes, trace gas and cloud condensation nuclei concentrations;
- Monitor soil moisture, precipitation, snowpack, stable water isotopes, and other hydrological variables to provide input and lateral boundary conditions for Earth-System models and as a basis for making more accurate water resource predictions for this and other semi-arid regions;

- Provide infrastructure for collaborative research among government laboratories, universities and private companies;
- Carry out intensive measurement campaigns;
- Provide training for undergraduate and graduate students and promote multidisciplinary research.

This article describes the Manitou Experimental Forest Observatory, presents on-going research at the site and highlights some initial findings. More specific scientific results and publications can be found in the publication list (Table S2) and within the individual articles as part of this special issue of Atmospheric Chemistry and Physics.

1.2 Site description and meteorological overview

The Manitou Experimental Forest (39.1006° N, 105.0942° W; Figure 1A,B), in the Front Range of the Colorado Rocky Mountains, has been managed as a research facility by the USDA Forest Service's Rocky Mountain Research Station since 1938. It contains approximately 6760 ha and exemplifies the Colorado Front Range wildland-urban interface where semi-arid montane forest ecosystems are in close proximity to larger urban centers. These interface areas, which also contain a number of small residential communities, are prone to wild fires from lightning as well as human causes. Two particularly large nearby fires (the 560 km^2 Hayman fire in 2002 and the 74 km^2 Waldo Canyon Fire in 2012) were among the most ecologically and economically damaging in the state's history. Although the primary study areas were not burned, areas within several km to the south and west of the site were affected by the 2002 fire. The landscape has thus been dramatically affected in both appearance and in the vegetation's ability to slow soil erosion from surface run-off during monsoon rains. Fire-damaged portions of the forest can change aspects of the atmospheric chemistry measured at the site through changes in gas- and

aerosol-phase emissions from nearby fire-scarred vegetation and soil. Wildfires are ubiquitous in the semi-arid forested American West, of which this area can be considered representative.

This forest's elevation ranges from 2,280 to 2,840 meters above sea level, and vegetation is primarily composed of forests of ponderosa pine, Douglas-fir, mixed conifer and aspen. The forest stands surrounding the observatory are relatively young, uneven-aged stands dominated by ponderosa pine. In 2009, core samples from a survey of 38 representative ponderosa pine showed that the median tree age was 49.5 years (with average, minimum and maximum ages of 62.5, 27, and 201 years respectively).

Soils underlying the tower site and the surrounding area are classified as deep, well-drained sandy loams and sandy gravelly loams originating from alluvial deposits weathered from underlying arkosic sandstone formations as well as nearby granite formations (Soil Conservation Service, 1992). Although numerous outcroppings of partially-weathered sandstone exist around the site, the average depth to bedrock is estimated to be between 1-1.8 m (36-60 inches) below ground surface. The soil ranges from slightly acidic to moderately alkaline (pH 6.1-7.8) with little organic matter content (1-4%) and rooting depths reported to be in excess of 1.3 m (40 inches). Soil permeability on undisturbed soils is moderately rapid (approx. 50-150 mm hr^{-1}). Rapid runoff generation and sediment transport occurs on compacted road surfaces, and other areas void of significant ground vegetation. The tower site is on an alluvial bench, formed by the erosion of underlying granite. It is situated in a broad, shallow valley approximately 1 km west of an intermittent creek, which flows towards the north. The terrain slope is asymmetric across this valley with the east side of the valley being steeper and the west side being more gradual (gradient between 3-8%).

The National Weather Service has been monitoring precipitation at MEF since 1940 (Station Woodland Park 8 NNW, Coop ID: 059210), and U.S. Forest Service staff have been collecting meteorological data including air and soil temperature, precipitation, and wind speed since 1998. The climate is cool (mean temperature is 19°C in July and -2°C in January) and dry with an average annual precipitation for 2010-2013 of 430.5 mm (16.94 inches). Approximately 50% of the precipitation falls as rain during the summer season (June – September) primarily during afternoon thunderstorms characterized by brief but intense periods of rainfall and lightning. Winter snowfall is typically light, and a persistent snowpack rarely develops.

Like much of Colorado, the site has a high frequency of sunny days during most of the year. During mid-day in July 2011, approximately 90% of the days had PAR values (photosynthetically active radiation between 400 and 700 nm) above the canopy that exceeded 2100 μmol m^{-2} s^{-1}, and part of every day reached a PAR value of at least 2000 μmol m^{-2} s^{-1}. Frequent afternoon thunderstorms can temporarily reduce the solar insolation, but rarely for more than three hours. Figure 2 shows the diel cycles of net longwave and shortwave radiation, latent heat flux, sensible heat flux and net CO_2 flux (calculated using the eddy covariance method) from four representative months during 2011. Each point represents the 30 minute average for that time period. The net radiation is calculated from the difference between the downwelling radiation and the upwelling radiation from the radiometers at the top (28 m) of the chemistry tower. It is interesting to note the net carbon uptake in the spring (April) and autumn (October) during the day, and the large nighttime respiration flux in July.

Numerous studies have been conducted here by researchers from a wide range of federal agencies, academic institutions, and non-governmental organizations. Early research focused on range management, including re-vegetation of abandoned fields, grazing management in native

and seeded pastures, watershed management in gully control, stream sedimentation, surface runoff, bacterial pollution, and infiltration (Gary et al., 1985). Recent research is more diverse, and includes a long-term (> 30 years) study on the flammulated owl (Linkhart et al., 2006, 2007), studies assessing the impacts of forest restoration and fuel reduction techniques (Battaglia et al., 2010, Massman et al., 2010, Rhoades et al., 2012), silviculture studies (Lezberg et al., 2008), and wildfire recovery studies (Fornwalt et al., 2010). Additional information about the site (including long-term weather, tree growth data and a bibliography of publications) can be found at: http://www.fs.usda.gov/manitou.

1.3 Measurements at the Manitou Experimental Forest Observatory (MEFO) under the auspices of BEACHON

In 2008, with cooperation with the USDA Forest Service, NCAR established the infrastructure at the site and named it the Manitou Experimental Forest Observatory (MEFO). The site includes four (4) mobile steel containers each having 160 ft^2 of laboratory floor space, numerous sampling ports, temperature-control and 20 kW power. Two research towers that extend through the canopy were constructed approximately 300 m apart (Figure 1C) and are referred to here as the micrometeorology and chemistry towers. Detailed information on these towers' measurements is listed in Table S1 in the supplementary materials section. A third (smaller) eddy-covariance measurement tower was deployed in a large clearing or 'forest gap' from 2011-2012. The purpose of this smaller tower was to make 4-way radiation measurements, surface skin temperature, and sensible and latent heat flux measurements over the grass and forb vegetation that is found beneath and in between the ponderosa pine. These measurements were taken at 1 and 3 m above ground level.

246 The micrometeorology tower (Figure 1E) is a narrow 45 m triangular tower (Rohn Products,
247 Peroria, IL, USA; model 45G; 425 mm per side) designed to facilitate the analysis of the impact
248 of canopy elements (needles, branches, trunks) on turbulent exchange between the surface,
249 canopy layers, and the overlying atmosphere. The instruments on the micrometeorology tower
250 operated nearly continuously from July 2009 until July 2012 when they were removed as a
251 precaution due the proximity of the Waldo Canyon Fire. This tower had instruments deployed at
252 six different levels (2, 8, 16, 22, 30, and 43 m), thus allowing several measurements within and
253 above the canopy (average canopy height ≈ 16 m). The 22 m level contained a 4-component
254 radiometer (Kipp and Zonen, The Netherlands, model CNR1) for measuring above-canopy
255 incoming and outgoing shortwave and longwave radiation. Instrumentation on the other five
256 levels included:

257 • Sonic anemometers (Campbell Scientific, Logan, UT, model CSAT3) to record the
258 three orthogonal wind velocity components and temperature fluctuations;
259 • NCAR-Vaisala (Vantaa, Finland) aspirated hygrothermometers to measure absolute
260 temperature and relative humidity;
261 • Open-path infrared gas analyzers (LiCOR, Lincoln, NE, model 7500) to measure
262 water vapor and carbon dioxide.

263 This multi-season dataset is being used to:

264 • Quantify the importance of canopy-induced modifications to turbulence in predicting
265 whole-ecosystem exchange in regional and global climate models,
266 • Partition water fluxes into transpiration and evaporation components, and
267 • Investigate impacts of spatially heterogeneous canopy distributions on evapotranspiration
268 using additional information from the chemistry and understory towers.

The chemistry tower is a 28 m walk-up type tower that is equipped with meteorological sensors as well as a variety of flux and gradient concentration measurements for gases and aerosols (Figure 1D). The platform on each level is 1.78 m × 1.27 m and is suitable for heavier instruments that require more space, power and maintenance. It can also support gradient sampling systems, which can move vertically along the tower. This tower is also equipped with 2D and 3D sonic anemometers, temperature, and radiation probes for continuous meteorological measurements and for calculating fluxes using the closed-path eddy covariance method. Other continuous gas-phase measurements from this tower have included: CO, CO_2, H_2O vapor, NO, NO_2 and SO_2. The Waldo Canyon fire in June 2012 forced the removal of the trace gas instruments from the chemistry tower and all of the instruments from the micrometeorological tower. Fortunately, the fire did not directly affect the site, and meteorological measurements from the chemistry tower have operated continuously (see Table S1). Since the two towers had generated 3-4 years of data and some of the instruments were required for other projects and field sites, it was decided to adjust the sampling strategy. Future core measurements of trace gases (CO, O3, SO2, NO_x) and aerosol number size distributions will be operated 4 times per year (for 4-6 weeks in duration) to capture the seasonal variability of these key species..

The suitability of these towers for making eddy covariance flux measurements in the surrounding landscape was analyzed by Kaser et al. (2013b). Briefly, the flux footprint was found to extend to 900 m for unstable boundary layer conditions and to 2500 m for stable conditions. However, because there is more heterogeneity in the forest composition and proximity to former burn areas inside the 2500 m radius, a practical limit of 1850 m beyond the tower was used as one of the criteria for valid flux data. A paved road ~ 500 m east of the tower site caused data to be eliminated if wind direction was from that sector.

The only significant woody vegetation around the observatory is ponderosa pine Measurements from this species include leaf- and branch-level photosynthesis, respiration and biogenic volatile organic compound (BVOC) emissions as well as sap flow using the compensation heat pulse method as described by Burgess et al. (2001). Leaf-level gas exchange was measured during peak sun exposure (9:00 – 14:00) on sunlit needles ~ 10m above the ground (Table 1). Each measurement was made on 6-10 mature needles, which were defined as needles that been on the branch through at least one winter. Gas exchange measurements were made using an LI-6400 portable gas exchange system (LI-COR Biosciences, Lincoln, NE) and photosynthesis, stomatal conductance, and transpiration calculations were made using total leaf area (measurement as described in Eller et al., 2013). The effects of high solar insolation, warm temperatures, and low humidity just prior to monsoon precipitation are demonstrated by the low stomatal conductance and photosynthesis values in July (Table 1).

Table 1: Mean values for needle-level gas exchange measured on mature *P. ponderosa* needles at the Manitou Experimental Forest Observatory. All calculations are based on total, rather than projected, leaf area. Values in parentheses give the range of measurement dates (2011 day of year). Standard deviations are given in italics (n=3).

	May (136-149)	June, July (178-185)	August (230-233)	September (263-265)
Net Phosynthesis (A) [μmol CO_2 m^{-2} s^{-1}]	2.9 *0.6*	0.9 *0.6*	3.2 *0.8*	3.5 *0.2*
Stomatal conductance(g_s) [mmol H_2O m^{-2} s^{-1}]	28 *9*	7 *5*	29 *12*	30 *6*
Transpiration [mmol H_2O m^{-2} s^{-1}]	0.49 *0.13*	0.35 *0.28*	1.00 *0.22*	0.64 *0.07*

A suite of hydrological measurements for total precipitation, soil moisture, leaf wetness and snow depth have been measured nearly continuously since 2009. Aerosol measurements include

two years (February 2010 to January 2012) of particle size distributions from 4 nm to 2.5 μm and 1 year of CCN (cloud condensation nuclei) data during March 2010 to April 2011 measured from one of the 4 mobile laboratories adjacent to the tower (Figure 1D). An additional month of CCN measurements (May 2011) was made above the canopy (25 m above ground) from the chemistry tower (Levin et al., 2012). BEACHON ROCS (Rocky Mountain Organics Study, 2010) and BEACHON RoMBAS (Rocky Mountain Biogenic Aerosol Study, 2011) were two large intensive measurement campaigns that occurred at the site. Selected results from these two campaigns as well as the initial 2008 Southern Rocky Mountain (SRM) study are discussed in this article and are summarized in Section 5. A more detailed summary of measurements at MEFO can be found in Table S1 in the Supplementary Material section. Campaign data and long-term observations are available at the following web site:

http://www2.acd.ucar.edu/campaigns

Other long-term data is available upon request from the corresponding author.

1.4 Meteorology at Manitou Experimental Forest Observatory

As mentioned in section 1.2, the observatory lies within a north-south drainage (draining to the north), leading to the formation of diurnal mountain-valley flows. Nighttime flow above the canopy (28 m) is dominated by drainage from the south as can be seen in Figures 3B and 3F. Winds below the canopy are often westerly or southwesterly due to drainage flow from surrounding ridgelines (Figure 3D). This height-dependent nocturnal pattern is dominant in all seasons. Daytime wind directions are much more variable. Although there is often a southerly flow during the day, other wind directions are also prevalent. Synoptic winter winds lead to a higher frequency of westerly and southwesterly flow (Figures 3A and 3E). These conditions tend to bring relatively unpolluted air to the site from the west. Stagnant high pressure

conditions lead to locally-induced upslope flow from either the northeast or southeast, which are consistently observed during daylight hours (Figure 3C). These periods are important in understanding the local chemistry as these flows transport air from Front Range cities (mainly Denver and Colorado Springs). Regardless of the daytime wind patterns, southerly drainage flow usually develops soon after the stable nocturnal boundary layer develops, which is often accompanied by an increase in anthropogenic pollutants. Wind measurements as well as modeling results suggest that this is often due to air from the Denver area during daytime upslope flow, which then drains towards the north and past the site at night.

2. Footprint hydrology in a water-limited ecosystem

2.1 Overview of hydrological measurements

Intensive hydrological measurements of total precipitation (rain and snow), soil moisture and snow depth as well as soil temperatures have been collected at MEFO since the summer of 2009. These complement the vertical flux measurements of water vapor for a complete accounting of the site's water budget. The precipitation measurements also augment the long-term records maintained by the USDA Forest Service mentioned in Section 1.2. A network of 11 tipping bucket rain gauges as well as an alter-shielded, weighing-type total precipitation gauge provide high time resolution, year-round precipitation measurements in a network distributed within the chemistry tower flux footprint in order to characterize the high spatial variability of precipitation. More details about these measurements are given in Table S1. The 2010-2013 annual accumulation of hourly precipitation is shown in Figure 4A. These time series are bias-corrected merged data products between the site's sensors in order to cover periodic data gaps. The site's annual precipitation measurements for a given year are defined by an end date of September 30 of that year and a start date of October 1 in the preceding year. The patterns

observed have been fairly consistent. Periodic precipitation episodes occur throughout the principal cool season of October through May followed by a brief dry season from late May through mid-June. This is followed by a summer period of rather intense precipitation episodes associated with the regional incursion of the North American Monsoon system. Finally there is an extended dry period starting in the late summer and extending into early autumn. The average annual accumulated precipitation for 2010-2013 was 430.5 mm with a range of 392 mm (in 2012) to 513 mm (in 2010). It should be noted that 2012 was among the driest years on record for most of Colorado, and the total precipitation for 2013 was similarly low. The latter year began with very low winter and spring snow fall, and stayed much drier than average until heavy September rains increased the total accumulated precipitation to about the same level observed in 2012. The maximum observed hourly rainfall recorded at the site from 2009-2013 was 57.9 mm, which occurred on Aug. 4, 2010. Other thunderstorms with high rain fall rates (up to 25 mm per hour) are common during the summer monsoon.

Seasonally-transient snowpack is an important feature of the hydrologic cycle as the snowpack can provide a lasting water source to the site during the spring melt period and can also insulate the soil from freezing temperatures. Snow depth measurements (Jenoptik, Inc., Jena, Germany, model SHM30 laser snow depth sensor) began during the winter of 2010-2011. Persistent patchy or complete snowpack is limited to December, January and February. Periodic snowstorms may also input appreciable moisture during the months of October, November, March and April although a snowpack rarely persists for more than 7 days.

Soil moisture probes (Decagon Devices, Pullman, WA, USA, model EC-5) and temperature profiles (Campbell Scientific, Logan, UT, USA, model T107 thermistors) extending from the near surface to approximately 1 meter depth are made at 3 different sites within the

micrometeorology tower's flux footprint. The merged annual cycle of soil moisture from all sites is shown in Figure 4B, and the annual soil temperature cycle is shown in Figure 4C. The soil moisture cycle exhibits some interesting and classic features of western landscape hydrology, especially the tendency for persistent dryness and pulsed recharge of near-surface moisture, particularly in the warm season. Deeper into the soil, the moisture variability is significantly damped and there is evidence of persistent soil moisture there, regardless of extended summer dry periods. This deeper layer of persistent wet soil helps sustain some of the total evaporative flux from the ponderosa pine ecosystem during the summer. There are extended periods of winter soil temperatures several degrees below 0 °C, which extends to approximately 70 cm below the surface. These low soil temperatures indicate that significant amounts of soil water freeze (i.e., creates 'soil frost') occasionally during the winter. The presence of soil frost is further evidenced by the sharp decline in recorded soil moisture values from December through late-February. Suppressed soil moisture values corresponding with sub-zero soil temperatures is a classic measurement artifact due to the significant change in soil dielectric permittivity as water undergoes phase change from liquid to ice and back again at the freezing point. This meltwater release and periodic melting of the transient snowpack impart additional water pulses to the site. As previously mentioned, MEFO typically experiences an early summer dry period before the onset of the monsoon rains, which is highly correlated with increased CO_2 and BVOC fluxes. The semi-arid climate creates very low mid-day stomatal conductance in ponderosa pine during the early- and late-summer dry periods (see Table 1), which protects the trees from water stress. When the monsoon rains start, these fluxes and stomatal conductance both increase substantially.

2.2 Water manipulation effects on ponderosa pine

Projected water limitations and higher temperatures are expected to put additional climate-induced physiological stresses on semi-arid forest ecosystems (Allen et al., 2010). To test hypotheses related to future climates, manipulation experiments must be carefully designed to ensure that data are representative of larger ecosystems responses (Beier et al., 2012). With these considerations in mind, another study at MEFO during 2010-2011 was designed to quantify the effect of different water treatments on the photosynthesis and respiration rates as well as BVOC emissions from mature trees (at least 10 m in height). Up to 50% of the incoming precipitation (snow and rain) was systematically diverted from the root zones (10 m × 10 m area) around targeted trees using an array of troughs (see iii in Figure 1C). The intercepted water was collected into barrels and then added to nearby trees resulting in a water continuum delivered to the various trees from 0.5 to 1.5 times the total precipitation such that the total amount of water delivered to the entire plot remained constant. Physiological parameters (e.g. sapflow, photosynthesis, and BVOC emissions) were measured on all trees within the experimental plot. Similar to the speciation seen in ambient air, branch-level measurements showed that the BVOCs emitted in the highest concentrations were methanol, 2-methyl-3-buten-2-ol, and monoterpenes. Initial observations showed that seasonality in plant physiological processes and weather dynamics interact to produce complex controls over climate-dependent emissions of these compounds with a strong dependence on soil moisture and precipitation. If the climate in this region shifts to a drier summer regime, total BVOCs emitted from needles of this forest are likely to decrease, which will have implications for modeling both gas- and liquid-phase regional chemistry. Studies such as this exemplify the interdisciplinary research questions addressed by

429 the BEACHON project, and are necessary to address the ecological system processes for
430 inclusion into Earth-System models as discussed in Section 1.1.
431
432 **3. Volatile organic compounds, oxidants and aerosol properties**
433 3.1 Volatile organic compound observations

434 Volatile organic compounds (VOCs) at MEFO are a mixture of biogenic and
435 anthropogenic compounds. The summertime VOC signals are dominated by biogenic emissions,
436 primarily methanol, ethanol, acetone, monoterpenes ($C_{10}H_{16}$, abbreviated by MT) and 2-methyl-
437 3-buten-2-ol ($C_5H_{10}O$, abbreviated by 232-MBO or MBO). Isoprene (C_5H_8) is also observed
438 during summer, but to a much lesser extent (~10-20% of 232-MBO concentrations).
439 Anthropogenic VOC concentrations are lower than the biogenic compounds and are typically
440 transported into the area from the Colorado Springs or Denver metropolitan areas.

441 A variety of techniques have been used to measure VOCs from different levels on the
442 chemistry tower, individual ponderosa pine branches, and from the ground. A quadrupole proton
443 transfer reaction mass spectrometer (PTR-MS; Ionicon, Analytik, Innsbruck, Austria) measured
444 a suite of selected VOCs (including methanol, acetonitrile, acetaldehyde, acetone+propanal, 232-
445 MBO+isoprene, benzene, monoterpenes and sesquiterpenes) during portions of each of the 2008-
446 2012 growing seasons. Under normal operating conditions, 232-MBO undergoes a dehydration
447 reaction in the PTR-MS drift tube leading to a molecular ion of m/z = 69. This is the same ion as
448 protonated isoprene, which is why they are reported as the sum of both species. Tower-based
449 measurements alternated between a six point gradient system (1.6, 5, 8.5, 12, 17.7 and 25.1 m
450 above ground) and an eddy covariance (EC) flux system at the top level (25.1 m). In addition, a
451 time-of-flight (TOF) PTR-MS (University of Innsbruck, Austria) was deployed for EC and

concentration measurements above the ponderosa pine canopy in 2010 and 2011 (Kaser et al., 2013a,b). A Selective Reagent Ion (SRI) PTR-TOF-MS (Ionicon Analytik, Innsbruck, Austria) instrument was used in 2011 to selectively distinguish 232-MBO from isoprene concentrations by using NO^+ as the reagent ion (Karl et al., 2012). This configuration was also used for one week in 2012 to continue these measurements for determining EC fluxes of 232 -MBO and isoprene (Karl et al., 2013). Figure 5 shows the vertical flux profiles for 232-MBO and total MT calculated from gradient measurements using the methodology described in Karl et al. (2004). It is evident that MBO emissions follow a light-dependent pattern and that the fluxes increase with height up to 12 m. MT emission patterns were vertically more uniformly distributed suggesting that the understory (forest litter, bark and trunks) also contributed to the total emissions. Using site-specific leaf cuvette measurements as model inputs, MEGAN 2.1 estimates showed good agreement with the measured average daytime 232-MBO + isoprene fluxes of 1.84 mg m^{-2} h^{-1}. After the large rain and hail storm on August 4th 2010 (which produced 57.9 mm precipitation in an hour; Section 2.1), monoterpene fluxes increased to 4.7 mg m^{-2} h^{-1} which is a factor 5-10 higher than what is normally observed (0.5-1mg m^{-2} h^{-1}) (Kaser et al., 2013b). Figure 6A shows the sum of MT and MBO+isoprene concentrations and fluxes starting on this day (August 4) and ending 1 week later (August 11). The increases in both emissions and fluxes, which continue for ~2 days after the rain event, are evident. The missing flux data on the first day (and periodically throughout the measurement period) are due to turbulence characteristics that are not amenable to EC calculations as described in section 1.3. The PTR-MS showed that ambient concentrations of several other BVOC (including cymene, camphor, nopinone, pinonaldehyde and sesquiterpenes) were also elevated after this vegetation disturbance.

The Trace Organic Gas Analyzer (TOGA, Apel et al., 2010) was deployed during the BEACHON ROCS campaign to measure concentrations of isoprene, 232-MBO, speciated MT and over 25 other targeted compounds. Results showed that the MT speciation is dominated by α-pinene, β-pinene and Δ-3-carene (approximately 25% each). Other quantified monoterpenes include camphene (7%), limonene (12%), myrcene (5%) and ocimene (1%). Figure 6B(1-4) shows August 2010 ambient diel concentrations of 4 selected VOCs reported by TOGA. The concentrations of the biogenic compounds MBO and MT are much higher than those of a typical anthropogenic compound (e.g. toluene) at this site, and the concentrations have different diurnal signatures. During the day, as the boundary layer grows and OH is present, MT concentrations are diminished even though their emissions are the greatest during this time. At night, the suppressed boundary layer height combined with decreased losses from O_3 and OH reactions leads to elevated MT concentrations that generally increase from 18:00 to midnight and remain elevated until 06:00-07:00. MBO emissions from ponderosa pine are strongly light dependent (Harley et al 1998, Kaser et al., 2013b) resulting in maximum emissions and ambient concentrations during midday with a secondary peak in early morning associated with initiation of emissions before the morning breakup of the nocturnal boundary layer. The combination of all 3 instruments used during BEACHON ROCS provided a unique opportunity to compare VOC measurement techniques under real-world conditions. The results were encouraging as the instruments agreed within ~20% for monoterpenes and ~10% for 232-MBO + isoprene with R^2 values of 0.85-0.97 (Kaser et. al. 2013a).

Consistent with ambient concentration measurements, branch- and needle-level BVOC emission measurements confirm the dominance of MBO in the emission profile; during daylight hours, MBO typically comprises >85% of the emitted reactive BVOC mass. Similar to ambient

observations, α-pinene, β-pinene, Δ-3-carene, camphene and limonene dominate the MT emissions, but a large number of other terpenoids are also emitted, including sabinene, myrcene, ocimene, α-terpinene, β-phellandrene, cymene, terpinolene, p-cymenene and the oxygenated monoterpenes linalool, terpineol and methyl chavicol. In many cases, especially in high light conditions, linalool was a major component of the leaf-level emissions. A number of sesquiterpenes, dominated by β-farnesene, also appear in emission samples. For model inputs, BVOC speciation is an important consideration as different compounds (such as MT isomers with the same chemical formula) have different reaction rate constants with OH, O_3 and NO_3, so their reaction products, pathways and atmospheric lifetimes can vary considerably. Additional soil BVOC flux measurements have been made using enclosures and a micrometeorological gradient technique at the site (Greenberg et al., 2012). These results suggested that emissions from the litter were negligible, contributing less than 1% of above-canopy emissions for all BVOCs measured.

A newly developed Thermal desorption Aerosol Gas chromatograph - Aerosol Mass Spectrometer (TAG-AMS) was deployed and used to analyze semi-volatile VOCs (~C_{14}-C_{25}) on a bihourly timescale. The sample collection, thermal desorption and chromatography systems have been described previously by Zhao et al. (2013), however the 2011 BEACHON-RoMBAS campaign was one of the first to couple it to the AMS as a detector (Williams et al., 2014). More than 70 semi-volatile gas-phase species were observed and quantified in the ambient atmosphere during the campaign. Source apportionment was used to identify the origin of these gas-phase species. Some were anthropogenic compounds (such as poly-aromatic hydrocarbons (PAH), oxygenated PAH and alkanes), but 23 species were identified to be terpenoid compounds of biogenic origin from a local source determined from Positive Matrix Factorization (PMF).

In addition to direct VOC emissions and transported species, it is also important to consider oxidation products. These compounds can influence tropospheric ozone formation, oxidative capacity of the atmosphere, and contribute to secondary organic aerosol. Concentrations and fluxes of two important oxygenated VOCs, formaldehyde (HCHO) and glyoxal (CHOCHO), were measured during the 2010 BEACHON-ROCS campaign (DiGangi et al., 2011, 2012) using Fiber Laser-Induced Fluorescence (FILIF; Hottle et al., 2009) and Laser-Induced Phosphorescence (Huisman et al., 2008). Ambient formaldehyde concentrations ranged between a minimum of ~0.5 ppb in the early morning hours (4:00 MST), and maximum values of 2-2.5 ppb in the evening (~20:00 MST). Ambient glyoxal concentrations ranged between a minimum of ~18 ppt in the early morning hours (6:00 MST), and maximum values of 30-55 ppt in the evening (~17:00 MST). The glyoxal:formaldehyde ratio maintained a stable diurnal cycle ratio with values of ~1.5-2% in the early morning and at night, and rising to ~2.5-3% in the middle of the days. In addition, to our knowledge, these canopy-scale HCHO eddy flux measurements are the first reported for any site. These results, coupled with enclosure measurements that showed minimal direct emissions, suggest a surprisingly large HCHO production source within the canopy air space. The mid-day HCHO fluxes were positive (upward) ranging from 37 to 131 $\mu g\ m^{-2}\ h^{-1}$ (see Figure 7b) and were correlated with temperature and radiation within the canopy. The missing HCHO source is thus consistent with oxidation of VOCs with light and temperature dependent emission profiles. The strength of HCHO fluxes cannot be accounted for by the oxidation of measured MBO and terpenes (also see section 3.2). A detailed analysis regarding HCHO sources and oxidation is discussed in DiGangi et al. (2011).

3.2 Peroxy and hydroxyl radical observations

Numerous studies (e.g. Stone et al., 2012) have highlighted discrepancies between modeled and measured radical concentrations in forested environments suggesting a lack of understanding of the chemical processes driving secondary pollutant formation. While most research has focused on regions dominated by isoprene emissions, results from several investigations indicate gaps in our understanding of BVOC oxidation in MBO- and monoterpene-dominated areas similar to MEFO (Kurpius and Goldstein, 2003; Day et al., 2008; Farmer and Cohen, 2008; Wolfe et al., 2011; Mao et al., 2012). Both the 2010 BEACHON-ROCS and 2011 BEACHON-ROMBAS campaigns included measurements of the hydroxyl radical (OH) and peroxy radicals (HO_2 and RO_2; see Table S1), using the techniques described by Edwards et al. (2003), Hornbrook et al. (2011) and Mauldin et al. (2001). This provided a unique opportunity to test our understanding of the chemical reactions that link BVOC oxidation with production of ozone and secondary organic aerosol (SOA) precursors.

Discrepancies between modeled and measured HO_x (= OH + HO_2) in regions with high BVOC levels have been primarily attributed to "missing" sources of OH (Thornton et al., 2002; Lelieveld et al., 2008; Hofzumahaus et al., 2009; Peeters et al., 2009). In the boundary layer, OH is produced both via "primary" sources, such as photolysis of ozone in the presence of water vapor, and via radical cycling reactions, such as reaction of HO_2 with NO.

$$O_3 + h\nu \rightarrow O(^1D) + O_2 \quad \text{(R1)}$$

$$O(^1D) + H_2O \rightarrow 2OH \quad \text{(R2)}$$

$$HO_2 + NO \rightarrow OH + NO_2 \quad \text{(R3)}$$

In a detailed analysis of OH observations, Kim et al. (2013) demonstrate that radical recycling via (R3) is likely the dominant source of OH within the MEFO canopy. A 0-D box model under-predicts HO_x concentrations relative to observations, implying unidentified sources of HO_2.

566 Using the same box model in a study focused on peroxy radical observations, Wolfe et al. (2013)
567 confirm this result and identify several potential additional sources of both HO_2 and RO_2.
568 Notably, it is suggested that oxidation of unmeasured, highly reactive BVOC could explain a
569 significant portion of the missing peroxy radical source. Such a source could also explain the
570 high HCHO fluxes observed during the same campaign (DiGangi et al, 2011; see Section 3.1).
571 Figure 7a compares the hourly-averaged measured and modeled total peroxy radical mixing
572 ratios for BEACHON-ROCS (August 2010). As described in Wolfe et al. (2013), the difference
573 between measured and modeled values corresponds to a total "missing" peroxy radical
574 production rate of as much as 130 ppt/min. For comparison, Figure 7b shows measured and
575 modeled HCHO fluxes (DiGangi et al., 2011). The additional HCHO production needed to
576 reconcile modeled and measured formaldehyde fluxes is on the order of 65 ppt/min at midday.
577 Uncertainties in measurements and model results contribute to a significant overall uncertainty in
578 these production rate estimates (approximately ± 50%). Nonetheless, the similarity between
579 these results—obtained via two essentially independent methods—supports the conclusion that
580 VOC oxidation within the canopy is much stronger than predicted by canonical chemical
581 mechanisms.

582 Analysis of the role of anthropogenic influence on the oxidation of BVOCs, especially
583 via the influence of NO_x on the fate of RO_2, is of great current interest (Orlando and Tyndall,
584 2012), and MEFO is well suited for such studies (see also section 4.1). Figure 8A shows the
585 measured HO_2, HO_2+RO_2, NO and NO_2 concentrations during a representative day in
586 BEACHON ROCS (August 24, 2010), and Figure 8C shows the corresponding wind speed and
587 direction. On this day, upslope conditions (that can bring polluted urban air and are often seen at
588 this site) were not observed, as the wind was generally out of the south or southwest where there

589 is relatively little anthropogenic influence. During the mid-morning as the boundary layer
590 developed, an increase in NO_x (Figure 8A) can be seen, which was likely due to downward
591 transport of a residual layer. The anthropogenic influence on the fate of RO_2 is evident as the
592 loss mechanism was initially dominated by the RO_2 + NO channel (Figure 8B), but during mid-
593 day as NO_x concentrations decreased (due to the residual morning boundary layer breaking up
594 and southwesterly flow to the site), the RO_2+HO_2 channel became the major loss mechanism.
595 While the patterns of these transitions do not appreciably affect the concentrations of biogenic
596 and anthropogenic VOCs, the changes in the role of the different reaction channels are consistent
597 with the measured HCHO and glyoxal concentrations (DiGangi et al., 2012) and measured and
598 modeled HO_2+RO_2 concentrations indicated in Figure 7. This competition between NO_x and
599 HO_2 for reaction with the peroxy radicals (RO_2) affects the composition of multigenerational
600 reaction products formed during gas-phase radical cycling and thus dictates, to a large extent, the
601 production of ozone and organic aerosol precursors.
602
603 3.3 Aerosol properties and composition
604 Particle size distribution measurements (covering diameters from 4 nm to 2.5 μm) were
605 conducted for nearly 2 years at MEFO starting in February 2010 and ending in January 2012.
606 The instruments used for these measurements consists of the following components:
607 • Optical Particle Counter (200 – 2500 nm); Lasair model 1002 from Particle
608 Measurement Systems (Boulder, CO, USA),
609 • Regular scanning mobility particle sizer (SMPS; 30-300 nm): Custom sheath air
610 and HV control unit combined with TSI model 3081 Differential Mobility

Analyzer (DMA) and TSI model 3760 Condensation Particle Counter (CPC; TSI Inc., Shoreview, MN, USA), and

- Nano SMPS (4-30 nm): Custom sheath air and HV control unit combined with TSI model 3085 DMA, and TSI model 3025a CPC.

Particle size distributions started at midnight at exact 5 minute intervals for a total of 288 size distributions per day. Frequent "small particle events" characterized by high concentrations of 4 – 20 nm particles were observed, especially during the summer season. The origin of these small particles is likely atmospheric nucleation (Kulmala et al., 2007), which is thought to be caused by reactions of gas-phase sulfuric acid with atmospheric bases such as ammonia and amines as well as oxidized organic compounds (Kirkby et al., 2011, Almeida et al., 2013). An example of three typical small particle events during July 2011 is shown in Figure 9A, where the onset of each event is seen just prior to noon (MST). These events are common at MEFO in the summer, occurring 3-5 times per week during late morning or early afternoon, and typically coincide with changes in wind speed and direction. Figure 9B shows wind speed and wind direction at the top of the chemistry tower and sulfate aerosol mass loadings measured by an aerosol mass spectrometer (described below). On each of these mornings the wind speed is fairly low (~1 m/s) at 8:00 MST with wind direction shifting from the south to a more northerly or northeasterly direction, indicating upslope transport from the Denver area. Thermal Desorption Chemical Ionization Mass Spectrometer (TDCIMS) measurements during these nucleation events demonstrated that sub-20 nm particles were composed of ~60% sulfate by mass whereas during non-event periods, sulfate contributed less than 40% of the mass to these small particles (Cui et al., 2014). In both event and non-event periods, the bulk aerosol mass is not significantly affected by this sulfate mass, as the majority of the total aerosol mass is

634 dominated by larger particles. The correlation with wind direction and the increase in sulfate
635 aerosol indicates that these events are anthropogenically induced, The scarcity of particles
636 smaller than 10 nm on July 29 suggests that nucleation is occurring away from the site, either
637 aloft (Mirme et al., 2010, Schobesberger,et al., 2013) or in the mixed layer shortly (~60 minutes
638 or less) upwind of the site.

639 A Fast Mobility Particle Sizer (FMPS, Model 3091, TSI Inc., Shoreview, MN, USA) was
640 used during BEACHON-RoMBAS to measure size-dependent particle fluxes (Pryor et al., 2013).
641 While the mean flux of both Aitken and nucleation mode particles was downwards, upward
642 fluxes were frequently observed. Based on quadrant and time-scale analyses using the University
643 of Helsinki Multicomponent Aerosol (UHMA) model (Korhonen et al., 2004), they found that
644 the upward fluxes of nucleation mode (< 30 nm diameter) particles were most strongly
645 influenced by upward transport of particle-rich air from the canopy resulting from the growth of
646 recently nucleated particles as well as coagulation processes. Downward fluxes of the Aitken
647 mode particles were more commonly linked to breakdown of the nocturnal inversion and
648 entrainment of particle-depleted air from above the canopy.

649 Average particle number concentrations at this site are usually less than 2×10^3 cm^{-3},
650 which is typical for rural continental environments, and concentrations rarely exceed 10^4 cm^{-3}.
651 During the August 2011 BEACHON-RoMBAS study, chemical speciation and mass loadings of
652 non-refractory PM_1 aerosol were measured using a high resolution time-of-flight aerosol mass
653 spectrometer (HR-ToF-AMS, Aerodyne Research, Inc., Billerica, MA; DeCarlo et al., 2006).
654 Average mass loadings during the campaign were 2.5 μg m^{-3} (Figure 10). Also included in this
655 figure is black carbon aerosol as measured with a single particle soot photometer (Droplet
656 Measurement Technologies, Boulder, CO, model SP2). Approximately 75% of the total PM_1

aerosol mass was comprised of organic aerosol (OA), with the rest composed primarily of ammonium sulfate. Nitrate concentrations were low and were shown to be primarily composed of organic nitrates (Fry et al., 2013). Black carbon (BC) aerosol mass was of the order of a few percent of the total submicron mass and more variable, often increasing and decreasing by an order of magnitude on hourly timescales. Transport from urban areas, fires, and local traffic likely explain this variability. Figure 10b shows the size-resolved composition for the same species and time period. Ammonium and sulfate size distributions were centered at 300-400 nm, while organics and nitrate aerosol size distributions were centered at ~250 nm. The distinct size distributions of the chemical components indicate that these aerosols are not completely internally mixed. Figure 10c shows the month-long daily distributions indicating a subtle diurnal cycle in organic aerosol, peaking at night, but with considerable day-to-day variability. The peak in average sulfate (and associated ammonium) at ~16:00-19:00 is primarily due to the influence of certain days where sulfate increased during late afternoon to early evening with corresponding SO_2 increases (see spikes in Figure 10a). The diurnal BC trends showed two peaks. The larger of these was in the evening (~20:00) coincident with the regular prolonged impact of the urban plume in afternoon through evening and was also seen in other anthropogenic species (e.g. NO_x, CO). The smaller, shorter-duration morning peak (~06:00 MST) was also correlated with NO_x and CO. The reason for this morning BC increase could be due to the break-up of the shallow nocturnal boundary layer causing mixing down of more pollution-rich residual layer air, or an increase of local emission sources into a shallow morning boundary layer. It should be noted that the diameter measured from BC aerosol is the mass equivalent diameter (D_{me}) which was obtained by assuming a density of 1.8 g cm^{-3} as recommended by Moteki et al. (2010). The aerodynamic diameter is estimated to be at least 1.8 times larger than the D_{me} shown in Figure

10b and could be larger than this if the BC was internally mixed with other non-BC compounds (e.g. organic coatings), or smaller if the particles had irregular shapes (DeCarlo et al., 2004).

$PM_{2.5}$ collection onto quartz fiber filters during the same campaign were analyzed for a variety of specific SOC (Secondary Organic Carbon) and carbon isotopic measurements as described in Geron (2011) and Lewandowski et al. (2013). These results estimated that 0.5 μgC m^{-3} could be attributed to specific SOC (Secondary Organic Carbon) precursors. Hemiterpene precursor compounds (isoprene + MBO) represented approximately half of the observed SOC, with monoterpenes contributing nearly the same amount to the total SOC. Isotopic measurements of these same filter samples found that the ^{14}C ratio was 0.71 ± 0.11 (range 0.52 to 0.88), indicating that roughly three quarters of the particulate carbon observed during BEACHON-RoMBAS was of modern, non-petrogenic origin. The fraction of modern carbon (70%) at this site is less than values observed in eastern U.S. forests. For example, Geron (2009) reported mean summer-time values of 83% and with maximum values reaching 97% for those forests. Similarly, during summer months near forests in the Eastern United States, Lewis et al. (2004) observed values between ~80-95%. Organic tracer results (including isoprene, MT, and 232-MBO oxidation products) indicate that the lower fraction of contemporary carbon is primarily due to lower total biogenic emissions and lower organic mass loadings and not due to more traffic or other urban influences (Kleindienst et al., 2007). The modern carbon results from MEFO can also be compared to measurements at nine Interagency Monitoring for Protection of Visual Environments (IMPROVE) network sites. The values from the urban sites in this network averaged approximately 50% (Bench et al., 2007).

Gas- and aerosol-phase organic nitrate concentrations were quantified with thermal dissociation, laser-included fluorescence (TD-LIF; Day et al., 2002, Rollins et al., 2010) during

summer 2011 (Fry et al., 2013). Gas-phase organic nitrate classes showed diurnal cycles peaking mid-day at ~200 ppt (total alkyl and multifunctional nitrates) ~300 ppt (total peroxy acyl nitrates) while total particle-phase organic nitrates peaked at night/early morning. Rates of formation of gas-phase organic nitrates within the shallow nocturnal boundary layer were comparable to daytime rates of formation. It was observed that total gas- and particle-phase organic nitrates had equilibrium-like responses to diurnal temperature changes, suggesting some reversible partitioning although thermodynamic modeling could not explain all of the repartitioning. Additionally, diurnal cycle of gas-particle partitioning supported modeled-predicted nighttime formation of lower volatility products, compared to daytime, from NO_3 radical-initiated oxidation of monoterpenes. Aerosol-phase organic nitrates were also measured by AMS and showed good agreement with TD-LIF (Fry et al., 2013).

Hundreds of acids in the gas and aerosol phases were quantified in real-time during summer 2011 using a newly-developed technique: the Micro-Orifice Volatilization Impactor High-Resolution Time-of-Flight Chemical Ionization Mass Spectrometer (MOVI-HRToF-CIMS; Yatavelli et al., 2012; 2014). It allowed for direct measurement of the gas-particle partitioning of individual and bulk organic acids. Comparisons to absorptive partitioning modeling demonstrated that bulk organic acids seemed to follow absorptive partitioning, responding to temperature changes on timescales of <1-2 hours, suggesting there were not major kinetic limitations to species evaporation. It was shown that species carbon number and oxygen content, together with ambient temperature, controlled the volatility of organic acids and are good predictors for partitioning. Moreover, the relationship between observed and model partitioning with carbon number and oxygen content pointed toward the likely importance of different classes of multifunctional organic acids that comprised the bulk of the acid groups (e.g. hydroxyacids,

hydroperoxyacids, or polyacids but not ketoacids).

A newly identified 232-MBO-derived organosulfate was identified in aerosol samples during BEACHON-RoMBAS, although at levels lower than reported for a previous California study (Zhang et al., 2012). The difference was tentatively attributed to the lower acidity of the pre-existing aerosol at BEACHON, as acidity is thought to greatly enhance the formation of this organosulfate. This species has the potential to be used as a tracer of SOA formation from 232-MBO.

Part of BEACHON-RoMBAS included the collection of time- and size-resolved biological aerosol properties. To our knowledge, this is the most extensive and comprehensive set of these measurements and data available. One key observation during the study was that rainfall events induced large increases in ambient fluorescent biological aerosol particle (FBAP) concentrations within the forest canopy (Huffman et al., 2013; Prenni et al., 2013), with concentrations remaining elevated for extended periods of time (> 12 hr) due to increased humidity and surface wetness. The largest observed increases, of more than an order of magnitude relative to dry conditions, occurred in the size range of 2-6 μm. Microscopic observations showed that these particles were dominated by biological cells at sizes with characteristics of bacterial aggregates and fungal spores (Huffman et al., 2013). Concentration increases that occurred during the rain events likely resulted from mechanical ejection of biological particles from surfaces (Constantinidou et al. 1990; Jones and Harrison, 2004), while a second, larger mode (which occurred after the rain) was likely actively emitted from biota on vegetated surfaces near the site (Elbert et al., 2007; Huffman et al., 2013). Contrary to the expectation that large particles will be washed out during precipitation, these data showed a significant increase in concentration and net upward flux of primary, super-micron particles after

749 rain, which demonstrates a direct and important link of airborne particles to the hydrological
750 cycle. Longer term measurements continued for ten months (July 2011 – June 2012) tracking the
751 seasonal FBAP cycle at the site and observing trends with season, precipitation and other
752 meteorological parameters (Schumacher et al., 2013).
753
754 3.4 Cloud condensation nuclei and ice nuclei
755 One of the primary goals of the BEACHON project was to determine the potential for
756 biogenic emissions to serve as CCN and ice nuclei (IN), which can impact cloud properties and
757 precipitation (e.g. Barth et al., 2005). It has been recently suggested that fungal spores may have
758 large influences on SOA formation in the Amazonian forest (Pöhlker et al., 2012), and as
759 discussed below, these biologically-influenced particles can influence both CCN and IN.
760 Changes in cloud properties and precipitation can, in turn, influence biogenic emissions, closing
761 the loop on a potentially important feedback between the carbon and water cycles (Pöschl et al,
762 2010, Morris et al., 2013).
763 To better understand the influence of biogenic secondary organic aerosol on aerosol
764 hygroscopicity and the seasonal variability of CCN, a continuous 14 month study (March 2010 -
765 May 2011) was performed at MEFO (Levin et al., 2012). This was followed by additional
766 measurements during the summer 2011 BEACHON-RoMBAS intensive campaign, which
767 allowed for direct comparison between aerosol hygroscopicity and aerosol chemical composition
768 measurements (Levin et al., 2013). Aerosol hygroscopicity was described using the
769 dimensionless hygroscopicity parameter, κ (Petters and Kreidenweis, 2007), showing an annual
770 averaged κ value of 0.16 ± 0.08. This value is similar to κ values measured in remote, forested
771 regions, such as in Finland (Cerully et al., 2011) and the Brazilian Amazon (Gunthe et al., 2009),

and is lower than the commonly assumed continental value of κ = 0.3 (Andreae and Rosenfeld, 2008). Aerosol composition derived from the hygroscopicity measurements at MEFO indicated a predominance of organic species in the aerosol, leading to the low κ measurement values. Direct comparison of organic mass fraction measured by aerosol mass spectrometry and filter measurements (discussed in Section 3.3) during BEACHON-RoMBAS agreed well with the composition derived from the hygroscopicity measurements. Organic mass fractions were found to be largest (up to 90%) in the smallest particles (20-30 nm as measured by the TDCIMS). This fraction decreased with increasing particle diameter as measured by the AMS (Figure 10B; Levin et al., 2013), and is consistent with the smallest particles being composed primarily of oxidized organic species from forest emissions. Results from the year-long measurements showed that κ was slightly higher during the winter months when biogenic emissions (which are strongly temperature-dependent) are suppressed. The combination of these results suggests that secondary organic aerosol derived from biogenic emissions impact aerosol hygroscopicity and CCN number concentrations throughout the year.

In addition to the CCN measurements, IN have also been characterized. Ice nucleating particles induce ice formation in clouds and are thought to be critical in initiating precipitation from mixed phase clouds (DeMott et al., 2010). During BEACHON-RoMBAS, IN number concentrations were characterized at temperatures between -34 ˚C and -9 ˚C. In addition, the particle sizes that induced freezing at temperatures greater than -20 ^{o}C were characterized via the droplet freezing technique. These particles as well as IN were both positively correlated with number concentrations of FBAP (Huffman et al., 2013; Prenni et al., 2013, Tobo et al., 2013). Similar to the precipitation-induced increases observed in biological particle concentrations, IN also increased during rain. The most dramatic example of this increase occurred on August 2,

2011, when a thunderstorm produced 19.6 mm of precipitation (maximum rainfall rate of 30 mm hr^{-1}). During this storm, IN concentrations at -25 °C increased from 2 L^{-1} to nearly 200 L^{-1} (Prenni et al., 2013). Correlation between IN and FBAP across the temperature range, coupled with DNA analysis of a portion of the residual IN, suggests that a significant fraction of the IN near the ground surface is composed of biological particles, particularly during and after rain events (Huffman et al., 2013, Prenni et al., 2013, Tobo et al., 2013). When lofted to altitudes where mixed-phase clouds persist, these biologically-influenced IN can influence subsequent precipitation, providing yet another feedback between biogenic emissions and the hydrologic cycle, and further linking the biosphere, hydrosphere and atmosphere.

4. Atmospheric processes at an urban-rural interface

4.1 Atmospheric chemistry

As mentioned in Section 2.2, the MEFO site is primarily influenced by clean continental air, but is periodically impacted by polluted air advected from the Colorado Front Range urban areas. This makes the site a suitable location to investigate interactions between biogenic and anthropogenic emissions, and a variety of interesting questions can be addressed. For example, how are the oxidation pathways of locally emitted BVOC influenced by oxidant levels (NO_3, OH and O_3) during clean and polluted conditions? In addition, to what extent does the transport of SO_2, oxidants and VOCs from urban areas affect particle nucleation and growth? Model simulations can be initialized and parameterized using long-term and campaign-specific measurements of aerosols, VOCs, trace gases, and meteorology. Results from these simulations can then be compared to observations. Local emissions are dominated by 232-MBO and monoterpenes, but these can be augmented by transport of anthropogenic species from the Front Range cities. Typical summertime ozone concentrations are 50-60 ppb during the afternoon, and

819 decrease to ~10-20 ppb at night. Nitrogen oxides (NO_x) are generally dominated by NO_2 with
820 typical values ~0.5 to 4.0 ppb, although occasional urban influences can cause the concentration
821 to increase to 8-10 ppb. NO concentrations are much lower – typically less than 0.5 ppb, and
822 rarely exceed 1.0 ppb. Since the area is relatively rural with low NO_x concentrations, ozone is
823 not titrated away at night as would typically happen in an urban environment. Average SO_2
824 concentrations are quite low year-round, averaging less than 0.2 ppb, but concentrations can
825 occasionally spike to ~2.0 ppb. The average August 2011 CO concentration was 123 ppb
826 (standard deviation of 27 ppb). These values increase when urban air is transported to the site,
827 but rarely exceed 150 ppb. Periodic CO measurements at other times of year have shown similar
828 consistent results. These direct measurements provide valuable insight into the range of
829 atmospheric conditions that the site experiences, and can be used as initial inputs and provide
830 constraints in modeling efforts. The relatively clean conditions combined with periodic, well-
831 defined urban perturbations make it an ideally situated location for studying atmospheric
832 processes at the rural-urban interface. An example of this was demonstrated in Figure 8 (adapted
833 from DiGangi et al., 2012), which shows the ambient concentrations of HO_2, RO_2, NO and NO_2
834 in 8A and the corresponding wind speed and direction in 8C during a representative BEACHON-
835 ROCS day (August 24, 2010). In the early morning, both HO_2 and RO_2 are very low (< 20 ppt),
836 accompanied by low wind speeds. During the day, the wind speed increases and becomes south-
837 easterly with an accompanying increase in NO (likely from the Colorado Springs area, ~40 km
838 SE of the site). At ~10:30 AM, there is an abrupt change in wind direction with air coming from
839 the SW (where there is little anthropogenic influence) accompanied by a sharp decrease in NO
840 concentrations. Concentrations of HO_2+RO_2 then reach maximum values during the early
841 afternoon at which point the HO_2 concentrations become maximized and the loss mechanism for

842 RO_2 is through the RO_2+HO_2 channel (Figure 8B). These observations demonstrate that the fate
843 of RO_2 radicals at the site is dominated by reaction with HO_2 under clean-air conditions and by
844 reaction with NO when influenced by urban air. The transitions between the two regimes can be
845 quite sharp, making the site well-suited for studying these types of transitions.
846
847 4.2 Coupled weather and chemistry modeling
848 Three-dimensional coupled meteorology and chemistry simulations of MEFO and the
849 surrounding region have been conducted using the Weather Research and Forecasting model
850 with chemistry (WRF-Chem; Grell et al., 2005, Fast et al., 2006). These model runs include gas-
851 phase and aerosol chemistry as well as aerosol effects on radiation and clouds. Simulations were
852 performed at 4 km horizontal grid spacing and compared to ground measurements during the
853 intensive BEACHON-ROCS and BEACHON-RoMBAS measurement periods. These modeling
854 studies focused particularly on organic aerosol (OA) formation from forest BVOC emissions,
855 and the influence of anthropogenic pollutants transported to the site. To study OA formation, the
856 WRF-Chem model was configured as described in Fry et al. (2013) using the SOA module based
857 on Hodzic and Jimenez (2011) for anthropogenic precursors and Shrivastava et al. (2011) for
858 biogenic precursors. To study the influence of anthropogenic pollution on aerosol formation, the
859 WRF-Chem model was configured as described in Cui et al. (2014). Back-trajectory
860 calculations based on WRF-Chem simulations confirm that these pollutants are advected from
861 the Front Range urban area (Figure 11). Elevated concentrations of NO_2 (and SO_2, not shown)
862 measured onsite coincide with the arrival of polluted air masses from Denver or Colorado
863 Springs, whereas low concentrations are associated with cleaner air advected from the west. The
864 effect of anthropogenic pollution on predicted OA composition suggests a fraction of modern

carbon that is of the order of that measured. Figure 12 shows that 30% or more of OA is influenced by anthropogenic species through either the formation of secondary organic aerosols by nighttime NO_3 chemistry, increased OH and O_3 oxidation, or the direct transport of anthropogenic OA to the site. NO_3 chemistry contributes to larger SOA concentrations at night when the boundary layer is shallow (Fry et al., 2013), but the overall contribution to the actual aerosol column relevant to radiative forcing is small (a 1 μg m^{-3} mass concentration represents a 100 μg m^{-2} column density in a 100 m nighttime boundary layer). Daytime aerosol mass loadings contribute much more to the regional aerosol mass due to the combination of the higher mass loadings and fully developed boundary layer (2 μg m^{-3} corresponds to 4000 μg m^{-2} in a 2 km daytime boundary layer; a forty-fold increase column height).

Small particle events (see section 3.3) were correlated with elevated SO_2 concentrations. Figure 13 shows the onset and subsequent growth of particles at the site during one of these events (July 29, 2011) as observed (panel a) and the corresponding WRF-Chem simulation (panel b). Model results indicate that initial particle formation is triggered by anthropogenic SO_2, whereas subsequent particle growth is driven by condensation of BVOC oxidation products (Cui et al., 2014) as discussed in section 3.3. Growth rates were calculated using the number mean diameter defined by (Matsui et al., 2011):

$$NMD = \frac{\sum_i Dp_i \times N_i}{\sum_i N_i} \quad (1)$$

where Dp_i and N_i are the diameter (nm) and number concentration respectively. The model simulations estimated that the average particle growth rates during these events (from 4-40 nm mobility diameter) were 3.4 nm hr^{-1}. The observed values calculated from SMPS measurements (average = 2.0 nm hr^{-1}) are less than the simulated values, but in reasonable agreement with other

reports from forested regions in Indiana, USA (2.5 nm hr^{-1}; Pryor et al., 2010) and Finland (2.9 nm hr^{-1}; Jaatinen et al., 2009). It should also be noted that there is considerable variability in reported growth rates, and this value is highly dependent upon the chosen diameter range.

The impact of biogenic aerosols on clouds and precipitation was also investigated as part of the BEACHON project. Figure 13c shows the effect of new particle formation on cloud condensation nuclei (CCN) concentrations at the site during 5 days in August 2011. The observed CCN concentrations are compared with the predicted values, computed with and without accounting for new particle formation in the model. These results show that modeled CCN concentration predictions (at 0.5% supersaturation) significantly under-predict the actual measured concentrations unless nucleation is taken into account. This demonstrates the importance of aerosol nucleation parameterization to accurately parameterize aerosol-cloud interactions. In future climate scenarios, it has been hypothesized that warmer temperatures (and potentially higher biogenic emissions) could have a negative climate feedback (Paasonen et al., 2013). This is because more oxidation products from BVOC emissions will be available for condensation, resulting in higher CCN concentrations and consequently increased cloud cover. Other regional modeling efforts utilizing BEACHON-ROCS and RoMBAS data are still underway to explore a variety of bio-hydro-atmosphere relationships.

5. Key findings from 2008-2011 field campaigns.

The Manitou Experimental Forest Observatory has hosted three multi-investigator intensive measurement campaigns, each designed to focus on specific aspects of bio-hydro-atmosphere interactions. Measurements made during the BEACHON-SRM08 (Southern Rocky

Mountains 2008) study provided an initial characterization of the site, provided data (specifically aerosol number and mass concentrations, CCN and hygroscopicity) for evaluation of regional-scale model simulations examining aerosol-cloud interactions, and enabled the identification of key scientific questions that could be addressed during subsequent field campaigns. The 2010 BEACHON-ROCS (Rocky Mountain Organic Carbon) study focused on BVOC oxidation and associated implications for oxidant cycling and distributions. The results showed that while there are compounds in the ambient air not typically measured by standard techniques, there is evidence that missing OH sinks are associated with oxidation products of known BVOC rather than primary emissions of unknown BVOC. The study also demonstrated that considerable BVOC oxidation takes place within the canopy air space. The following year (2011) the BEACHON-RoMBAS (Rocky Mountain Biogenic Aerosol Study) took place to characterize a multitude of aerosol processes at the site and incorporate the findings from the gas-phase measurements of BEACHON-ROCS into modeling efforts. Among the many measurements performed were IN, CCN, particle size distributions, chemical speciation of bulk aerosol and small (<30 nm) particles, gas- and particle-phase partitioning, black carbon, elemental:organic carbon (EC:OC) ratios, gas-phase nitrate and NO_x, and super-micron biological particles. This campaign also included many of the same gas-phase measurements from 2010 to further characterize BVOC emissions, oxidant levels and oxidation products. Many of the long-term seasonal observations (see Table S1) have been valuable in characterizing the site, and for interpreting measurements taken during the intensive measurement campaigns. Table S2 in the supplementary materials section lists the publication results from the past 5 years based on MEFO observations. Future investigations and data analysis from past measurements are expected to result in further publications, additional observations, and more collaborative

research. This is not intended to be an exhaustive list, but rather provide context for the research site and further information for past, present and future researchers.

6. Conclusion

Observations at the Manitou Experimental Forest Observatory have provided important data for understanding terrestrial-atmosphere interactions in a semi-arid ponderosa pine forest that is typical of the Colorado Front Range urban-rural interface. Studies of biogenic emissions and their influence on gas-phase chemistry, aerosol properties and cloud condensation nuclei have led to a number of interesting conclusions – some of which have been summarized herein. High-frequency turbulence measurements coupled with corresponding CO_2, water, and energy fluxes at the site are now being incorporated into the land-surface schemes of climate models to more accurately represent canopy influences. The unique observational data are available for other model parameterization and evaluation studies. The infrastructure exists to enable additional measurements and future scientific measurement campaigns as well as for testing new instruments, measurement inter-comparisons, graduate and undergraduate student development and other studies involving terrestrial-atmospheric exchange processes. MEFO is a collaborative facility that is maintained through a cooperative agreement between NCAR and the USDA Forest Service and is available to the scientific community for training, model development and evaluation and scientific discovery.

Acknowledgments

The authors would like to acknowledge generous field support from Richard Oakes (USDA Forest Service, Manitou Experimental Forest Site Manager). Authors from Colorado State University were supported through NSF grant ATM-0919042. Authors from the University of

955 Colorado were supported by NSF grant ATM-0919189 and United States Department of Energy
956 grant DE-SC0006035. Authors from the National Center for Atmospheric Research were
957 supported by NSF grant ATM-0919317 and U. S. Department of Energy grant DE-SC00006861.
958 Thomas Karl was also supported by the EC Seventh Framework Program (Marie Curie
959 Reintegration Program, "ALP-AIR", grant no. 334084). S. C. Pryor (Indiana University) was
960 supported by NSF ATM-1102309. Authors from the University of Innsbruck were supported by
961 the Austrian Science Fund (FWF) under the project number L518-N20. L. Kaser was also
962 supported from a DOC-fFORTE-fellowship of the Austrian Academy of Science. Authors from
963 the University of Wisconsin-Madison were supported by NSF grant ATM-0852406, the
964 BEACHON project and NASA-SBIR Phase I & II funding. Contributions from Los Alamos
965 National Laboratory (LANL) were funded by the United States Department of Energy's
966 Atmospheric System Research (Project F265, KP1701, M.K. Dubey principal investigator).
967 A.C. Aiken also thanks LANL - Laboratory Directed Research and Development for a Director's
968 postdoctoral fellowship award. The authors would also like to acknowledge substantial
969 participation and input from the Max Planck Institute for Chemistry (MPIC; Mainz, Germany),
970 which was funded by the Max Planck Society (MPG) and the Geocycles Cluster Mainz (LEC
971 Rheinland-Pfalz). J. A. Huffman acknowledges internal faculty support from the University of
972 Denver. The United States Environmental Protection Agency (EPA), through its Office of
973 Research and Development, collaborated in the research described here. The manuscript has
974 been subjected to peer review and has been cleared for publication by the EPA. Mention of trade
975 names or commercial products does not constitute endorsement or recommendation for use. The
976 National Center for Atmospheric Research is sponsored by the National Science Foundation.
977 Any opinions, findings and conclusions or recommendations expressed in the publication are

those of the authors and do not necessarily reflect the views of the National Science Foundation or the U.S. Environmental Protection Agency.

References

Allen, C. D., Macalady, A. K., Chenchouni, H., Bachelet, D., McDowell, N., Vennetier, M., Kitzberger, T., Rigling, A., Breshears, D. D., Hogg, E. H., Gonzalez, P., Fensham, R., Zhang, Z., Castro, J., Demidova, N., Lim, J. H., Allard, G., Running, S. W., Semerci, A., and Cobb, N.: A global overview of drought and heat-induced tree mortality reveals emerging climate change risks for forests, Forest Ecol. Manag., 259, 660-684, 10.1016/j.foreco.2009.09.001, 2010.

Almeida, J., Schobesberger, S., Kurten, A., Ortega, I. K., Kupiainen-Maatta, O., Praplan, A. P., Adamov, A., Amorim, A., Bianchi, F., Breitenlechner, M., David, A., Dommen, J., Donahue, N. M., Downard, A., Dunne, E., Duplissy, J., Ehrhart, S., Flagan, R. C., Franchin, A., Guida, R., Hakala, J., Hansel, A., Heinritzi, M., Henschel, H., Jokinen, T., Junninen, H., Kajos, M., Kangasluoma, J., Keskinen, H., Kupc, A., Kurten, T., Kvashin, A. N., Laaksonen, A., Lehtipalo, K., Leiminger, M., Leppa, J., Loukonen, V., Makhmutov, V., Mathot, S., McGrath, M. J., Nieminen, T., Olenius, T., Onnela, A., Petaja, T., Riccobono, F., Riipinen, I., Rissanen, M., Rondo, L., Ruuskanen, T., Santos, F. D., Sarnela, N., Schallhart, S., Schnitzhofer, R., Seinfeld, J. H., Simon, M., Sipila, M., Stozhkov, Y., Stratmann, F., Tome, A., Trostl, J., Tsagkogeorgas, G., Vaattovaara, P., Viisanen, Y., Virtanen, A., Vrtala, A., Wagner, P. E., Weingartner, E., Wex, H., Williamson, C., Wimmer, D., Ye, P. L., Yli-Juuti, T., Carslaw, K. S., Kulmala, M., Curtius, J., Baltensperger, U., Worsnop, D. R., Vehkamaki, H., and Kirkby, J.: Molecular understanding of sulphuric acid-amine particle nucleation in the atmosphere, Nature, 502, 359-+, 10.1038/nature12663, 2013.

Alo, C. A., and Wang, G. L.: Hydrological impact of the potential future vegetation response to climate changes projected by 8 GCMs, Journal of Geophysical Research-Biogeosciences, 113, 16, 10.1029/2007jg000598, 2008.

Andreae, M. O., and Rosenfeld, D.: Aerosol-cloud-precipitation interactions. Part 1. The nature and sources of cloud-active aerosols, Earth Sci. Rev., 89, 13-41, 10.1016/j.earscirev.2008.03.001, 2008.

Apel, E. C., Emmons, L. K., Karl, T., Flocke, F., Hills, A. J., Madronich, S., Lee-Taylor, J., Fried, A., Weibring, P., Walega, J., Richter, D., Tie, X., Mauldin, L., Campos, T., Weinheimer, A., Knapp, D., Sive, B., Kleinman, L., Springston, S., Zaveri, R., Ortega, J., Voss, P., Blake, D., Baker, A., Warneke, C., Welsh-Bon, D., de Gouw, J., Zheng, J., Zhang, R., Rudolph, J., Junkermann, W., and Riemer, D. D.: Chemical evolution of volatile organic compounds in the outflow of the Mexico City Metropolitan area, Atmos. Chem. Phys., 10, 2353-2375, 2010.

Barth, M., McFadden, J. P., Sun, J. L., Wiedinmyer, C., Chuang, P., Collins, D., Griffin, R., Hannigan, M., Karl, T., Kim, S. W., Lasher-Trapp, S., Levis, S., Litvak, M., Mahowald, N., Moore, K., Nandi, S., Nemitz, E., Nenes, A., Potosnak, M., Raymond, T. M., Smith, J., Still, C., and Stroud, C.: Coupling between land ecosystems and the atmospheric hydrologic cycle through

biogenic aerosol pathways, B. Am. Meterol. Soc., 86, 1738-1742, 10.1175/bams-86-12-1738, 2005.

Battaglia, M. A., Rocca, M. E., Rhoades, C. C., and Ryan, M. G.: Surface fuel loadings within mulching treatments in Colorado coniferous forests, Forest Ecol. Manag., 260, 1557-1566, 10.1016/j.foreco.2010.08.004, 2010.

Beier, C., Beierkuhnlein, C., Wohlgemuth, T., Penuelas, J., Emmett, B., Korner, C., de Boeck, H. J., Christensen, J. H., Leuzinger, S., Janssens, I. A., and Hansen, K.: Precipitation manipulation experiments - challenges and recommendations for the future, Ecol. Lett., 15, 899-911, 10.1111/j.1461-0248.2012.01793.x, 2012.

Bench, G., Fallon, S., Schichtel, B., Malm, W., and McDade, C.: Relative contributions of fossil and contemporary carbon sources to PM 2.5 aerosols at nine Interagency Monitoring for Protection of Visual Environments (IMPROVE) network sites, Journal of Geophysical Research-Atmospheres, 112, 10, 10.1029/2006jd007708, 2007.

Berkelhammer, M., Hu, J., Bailey, A., Noone, D.C. Still, C. Barnard, H. Gochis, D., Hsiao, G.S. Rahn, T., and Turnipseed, A.: The nocturnal water cycle in an open-canopy forest. J. Geophys. Res-Atmos., DOI: 10.1002/jgrd.50701, 2013.

Burgess, S. S. O., Adams, M. A., Turner, N. C., Beverly, C. R., Ong, C. K., Khan, A. A. H., and Bleby, T. M.: An improved heat pulse method to measure low and reverse rates of sap flow in woody plants, Tree Physiol., 21, 589-598, 2001.

Carslaw, K. S., Boucher, O., Spracklen, D. V., Mann, G. W., Rae, J. G. L., Woodward, S., and Kulmala, M.: A review of natural aerosol interactions and feedbacks within the Earth system, Atmospheric Chemistry and Physics, 10, 1701-1737, 10.5194/acp-10-1701-2010, 2010.

Cerully, K. M., Raatikainen, T., Lance, S., Tkacik, D., Tiitta, P., Petaja, T., Ehn, M., Kulmala, M., Worsnop, D. R., Laaksonen, A., Smith, J. N., and Nenes, A.: Aerosol hygroscopicity and CCN activation kinetics in a boreal forest environment during the 2007 EUCAARI campaign, Atmos. Chem. Phys., 11, 12369-12386, 10.5194/acp-11-12369-2011, 2011.

Constantinidou, H.A., Hirano, S.S., Baker, L.S., Upper, C.D.: Atmospheric dispersal of ice nucleation-active bacteria: The role of rain. Phytopathology, 80, 934-937, 1990.

Cross, E. S., Hunter, J. F., Carrasquillo, A. J., Franklin, J. P., Herndon, S. C., Jayne, J. T., Worsnop, D. R., Miake-Lye, R. C., and Kroll, J. H.: Online measurements of the emissions of intermediate-volatility and semi-volatile organic compounds from aircraft, Atmospheric Chemistry and Physics, 13, 7845-7858, 10.5194/acp-13-7845-2013, 2013.

Cui, Y. Y., Hodzic, A., Smith, J. N., Ortega, J., Brioude, J., Matsui, H., Turnipseed, A., Winkler, P., and de Foy, B.: Modeling ultrafine particle growth at a pine forest site influenced by

anthropogenic pollution during BEACHON-RoMBAS 2011, Atmos. Chem. Phys. Discuss., 14, 5611-5651, doi:10.5194/acpd-14-5611-2014, 2014

Day, D. A., Wooldridge, P. J., and Cohen, R. C.: Observations of the effects of temperature on atmospheric HNO3, Sigma ANs, Sigma PNs, and NOx: evidence for a temperature-dependent HOx source, Atmospheric Chemistry and Physics, 8, 1867-1879, 2008.

Day, D. A., Wooldridge, P. J., Dillon, M. B., Thornton, J. A., and Cohen, R. C.: A thermal dissociation laser-induced fluorescence instrument for in situ detection of NO2, peroxy nitrates, alkyl nitrates, and HNO3, Journal of Geophysical Research-Atmospheres, 107, 14, 10.1029/2001jd000779, 2002.

DeCarlo, P. F., Kimmel, J. R., Trimborn, A., Northway, M. J., Jayne, J. T., Aiken, A. C., Gonin, M., Fuhrer, K., Horvath, T., Docherty, K. S., Worsnop, D. R., and Jimenez, J. L.: Field-deployable, high-resolution, time-of-flight aerosol mass spectrometer, Analytical Chemistry, 78, 8281-8289, 10.1021/ac061249n, 2006.

DeMott, P. J., and Prenni, A. J.: New Directions: Need for defining the numbers and sources of biological aerosols acting as ice nuclei, Atmospheric Environment, 44, 1944-1945, 10.1016/j.atmosenv.2010.02.032, 2010.

DeMott, P. J., Prenni, A. J., Liu, X., Kreidenweis, S. M., Petters, M. D., Twohy, C. H., Richardson, M. S., Eidhammer, T., and Rogers, D. C.: Predicting global atmospheric ice nuclei distributions and their impacts on climate, Proceedings of the National Academy of Sciences of the United States of America, 107, 11217-11222, 10.1073/pnas.0910818107, 2010.

Denman, K.L., Brasseur, G., Chidthaisong, A., Ciais, P., Cox, P. M., Dickinson, R.E., Hauglustaine, D., Heinze, C., Holland, E., Jacob, D., Lohmann, U., Ramachandran, S., da Silva Dias, P. L., Wofsy, S. C., Zhang, X.: Couplings Between Changes in the Climate System and Biogeochemistry. In: Climate Change 2007: The Physical Science Basis. Contribution of Working Group I to the Fourth Assessment Report of the Intergovernmental Panel on Climate Change [Solomon, S., D. Qin, M. Manning, Z. Chen, M. Marquis, K.B. Averyt, M.Tignor and H.L. Miller (eds.)]. Cambridge University Press, Cambridge, United Kingdom and New York, NY, USA, 2007.

DiGangi, J. P., Boyle, E. S., Karl, T., Harley, P., Turnipseed, A., Kim, S., Cantrell, C., Maudlin, R. L., Zheng, W., Flocke, F., Hall, S. R., Ullmann, K., Nakashima, Y., Paul, J. B., Wolfe, G. M., Desai, A. R., Kajii, Y., Guenther, A., and Keutsch, F. N.: First direct measurements of formaldehyde flux via eddy covariance: implications for missing in-canopy formaldehyde sources, Atmos. Chem. Phys., 11, 10565-10578, 10.5194/acp-11-10565-2011, 2011.

DiGangi, J. P., Henry, S. B., Kammrath, A., Boyle, E. S., Kaser, L., Schnitzhofer, R., Graus, M., Turnipseed, A., Park, J. H., Weber, R. J., Hornbrook, R. S., Cantrell, C. A., Maudlin, R. L., Kim, S., Nakashima, Y., Wolfe, G. M., Kajii, Y., Apel, E. C., Goldstein, A. H., Guenther, A., Karl, T.,

Hansel, A., and Keutsch, F. N.: Observations of glyoxal and formaldehyde as metrics for the anthropogenic impact on rural photochemistry, Atmos. Chem. Phys., 12, 9529-9543, 10.5194/acp-12-9529-2012, 2012.

Dube, W. P., Brown, S. S., Osthoff, H. D., Nunley, M. R., Ciciora, S. J., Paris, M. W., McLaughlin, R. J., and Ravishankara, A. R.: Aircraft instrument for simultaneous, in situ measurement of NO3 and N2O5 via pulsed cavity ring-down spectroscopy, Review of Scientific Instruments, 77, 11, 10.1063/1.2176058, 2006.

Edwards, G. D., Cantrell, C. A., Stephens, S., Hill, B., Goyea, O., Shetter, R. E., Mauldin, R. L., Kosciuch, E., Tanner, D. J., and Eisele, F. L.: Chemical ionization mass spectrometer instrument for the measurement of tropospheric HO_2 and RO_2, Analytical Chemistry, 75, 5317-5327, 10.1021/ac034402b, 2003.

Eisele, F. L., and Tanner, D. J.: ION-ASSISTED TROPOSPHERIC OH MEASUREMENTS, Journal of Geophysical Research-Atmospheres, 96, 9295-9308, 10.1029/91jd00198, 1991.

Eisele, F. L., and Tanner, D. J.: MEASUREMENT OF THE GAS-PHASE CONCENTRATION OF H2SO4 AND METHANE SULFONIC-ACID AND ESTIMATES OF H2SO4 PRODUCTION AND LOSS IN THE ATMOSPHERE, Journal of Geophysical Research-Atmospheres, 98, 9001-9010, 10.1029/93jd00031, 1993.

Elbert, W., Taylor, P. E., Andreae, M. O., and Poschl, U.: Contribution of fungi to primary biogenic aerosols in the atmosphere: wet and dry discharged spores, carbohydrates, and inorganic ions, Atmos. Chem. Phys., 7, 4569-4588, 2007.

Eller, A. S. D., Harley, P., and Monson, R. K.: Potential contribution of exposed resin to ecosystem emissions of monoterpenes, Atmospheric Environment, 77, 440-444, 2013.

Farmer, D. K., and Cohen, R. C.: Observations of HNO3, Sigma AN, Sigma PN and NO2 fluxes: evidence for rapid HOx chemistry within a pine forest canopy, Atmospheric Chemistry and Physics, 8, 3899-3917, 2008.

Fast, J. D., Gustafson, W. I., Easter, R. C., Zaveri, R. A., Barnard, J. C., Chapman, E. G., Grell, G. A., and Peckham, S. E.: Evolution of ozone, particulates, and aerosol direct radiative forcing in the vicinity of Houston using a fully coupled meteorology-chemistry-aerosol model, J. Geophys. Res-Atmos., 111, 10.1029/2005jd006721, 2006.

Fornwalt, P. J., Kaufmann, M. R., and Stohlgren, T. J.: Impacts of mixed severity wildfire on exotic plants in a Colorado ponderosa pine-Douglas-fir forest, Biol. Invasions, 12, 2683-2695, 10.1007/s10530-009-9674-2, 2010.

Fry, J. L., Draper, D. C., Zarzana, K. J., Campuzano-Jost, P, Day, D. A., Jimenez, J. L., Brown, S. S., Cohen, R. C., Kaser, L., Hansel, A., Cappellin, L., Karl, T., Hodzic-Roux, A., Turnipseed,

A., Cantrell, C., Lefer, B. L., and Grossberg, N.: Observations of gas- and aerosol-phase organic nitrates at BEACHON-RoMBAS 2011, Atmos. Chem. Phys., 13, 8585-8605, 2013.

Gary, H. L.: A summary of research at the Manitou Experimental Forest in Colorado, 1937-1983. U.S. Department of Agriculture, Forest Service Publication, Rocky Mountain Forest and Range Experiment Station, Fort Collins, CO, 1985.

Geron, C.: Carbonaceous aerosol over a Pinus taeda forest in Central North Carolina, USA, Atmospheric Environment, 43, 959-969, 10.1016/j.atmosenv.2008.10.053, 2009.

Geron, C.: Carbonaceous aerosol characteristics over a Pinus taeda plantation: Results from the CELTIC experiment, Atmospheric Environment, 45, 794-801, 10.1016/j.atmosenv.2010.07.015, 2011.

Greenberg, J. P., Asensio, D., Turnipseed, A., Guenther, A. B., Karl, T., and Gochis, D.: Contribution of leaf and needle litter to whole ecosystem BVOC fluxes, Atmos. Environ., 59, 302-311, 10.1016/j.atmosenv.2012.04.038, 2012.

Grell, G. A., Peckham, S. E., Schmitz, R., McKeen, S. A., Frost, G., Skamarock, W. C., and Elder, B.: Fully coupled "online" chemistry within the WRF model, Atmos. Environ., 39, 37, 6957-6975, DOI: 10.1016/j.atmosenv.2005.04.027, 2005.

Guenther, A., Kulmala, M., Turnipseed, A., Rinne, J., Suni, T., and Reissell, A.: Integrated land ecosystem-atmosphere processes study (iLEAPS) assessment of global observational networks, Boreal Environ. Res., 16, 321-336, 2011.

Gunthe, S. S., King, S. M., Rose, D., Chen, Q., Roldin, P., Farmer, D. K., Jimenez, J. L., Artaxo, P., Andreae, M. O., Martin, S. T., and Poschl, U.: Cloud condensation nuclei in pristine tropical rainforest air of Amazonia: size-resolved measurements and modeling of atmospheric aerosol composition and CCN activity, Atmos. Chem. Phys., 9, 7551-7575, 2009.

Haman, C. L., Lefer, B., and Morris, G. A.: Seasonal Variability in the Diurnal Evolution of the Boundary Layer in a Near-Coastal Urban Environment, Journal of Atmospheric and Oceanic Technology, 29, 697-710, 10.1175/jtech-d-11-00114.1, 2012.

Harley, P., Fridd-Stroud, V., Greenberg, J., Guenther, A., and Vasconcellos, P.: Emission of 2-methyl-3-buten-2-ol by pines: A potentially large natural source of reactive carbon to the atmosphere, Journal of Geophysical Research-Atmospheres, 103, 25479-25486, 10.1029/98jd00820, 1998.

Heald, C. L., Wilkinson, M. J., Monson, R. K., Alo, C. A., Wang, G. L., and Guenther, A.: Response of isoprene emission to ambient CO2 changes and implications for global budgets, Global Change Biology, 15, 1127-1140, 10.1111/j.1365-2486.2008.01802.x, 2009.

Hodzic, A., and Jimenez, J. L.: Modeling anthropogenically controlled secondary organic aerosols in a megacity: a simplified framework for global and climate models, Geoscientific Model Development, 4, 901-917, 10.5194/gmd-4-901-2011, 2011.

Hoffmann, T., Bandur, R., Hoffmann, S., and Warscheid, B.: On-line characterization of gaseous and particulate organic analytes using atmospheric pressure chemical ionization mass spectrometry, Spectrochimica Acta Part B-Atomic Spectroscopy, 57, 1635-1647, 10.1016/s0584-8547(02)00111-8, 2002.

Hofzumahaus, A., Rohrer, F., Lu, K. D., Bohn, B., Brauers, T., Chang, C. C., Fuchs, H., Holland, F., Kita, K., Kondo, Y., Li, X., Lou, S. R., Shao, M., Zeng, L. M., Wahner, A., and Zhang, Y. H.: Amplified Trace Gas Removal in the Troposphere, Science, 324, 1702-1704, 10.1126/science.1164566, 2009.

Hornbrook, R. S., Crawford, J. H., Edwards, G. D., Goyea, O., Mauldin, R. L., Olson, J. S., and Cantrell, C. A.: Measurements of tropospheric HO_2 and RO_2 by oxygen dilution modulation and chemical ionization mass spectrometry, Atmospheric Measurement Techniques, 4, 735-756, 10.5194/amt-4-735-2011, 2011.

Hottle, J. R., Huisman, A. J., Digangi, J. P., Kammrath, A., Galloway, M. M., Coens, K. L., Keutsch, F. N.: A Laser Induced Fluorescence-Based Instrument for In-Situ Measurements of Atmospheric Formaldehyde, Environmental Science & Technology, 43, 3, 790-795, 10.1021/es801621f, 2009.

Huffman, J. A., Docherty, K. S., Aiken, A. C., Cubison, M. J., Ulbrich, I. M., DeCarlo, P. F., Sueper, D., Jayne, J. T., Worsnop, D. R., Ziemann, P. J., and Jimenez, J. L.: Chemically-resolved aerosol volatility measurements from two megacity field studies, Atmospheric Chemistry and Physics, 9, 7161-7182, 2009.

Huffman, J. A., Prenni, A. J., DeMott, P. J., Pohlker, C., Mason, R. H., Robinson, N. H., Frohlich-Nowoisky, J., Tobo, Y., Despres, V. R., Garcia, E., Gochis, D. J., Harris, E., Mueller-Germann, I., Ruzene, C., Schmer, B., Sinha, B., Day, D. A., Andreae, M. O., Jimenez, J. L., Gallagher, M., Kreidenweis, S. M., Bertram, A. K., and Poschl, U.: High concentrations of biological aerosol particles and ice nuclei during and after rain, Atmos. Chem. Phys., 13, 6151-6164, 10.5194/acp-13-6151-2013, 2013.

Huisman, A. J., Hottle, J. R., Coens, K. L., DiGangi, J. P., Galloway, M. M., Kammrath, A., and Keutsch, F. N.: Laser-induced phosphorescence for the in situ detection of glyoxal at part per trillion mixing ratios, Analytical Chemistry, 80, 5884-5891, 10.1021/ac800407b, 2008.

Jaatinen, A., Hamed, A., Joutsensaari, J., Mikkonen, S., Birmili, W., Wehner, B., Spindler, G., Wiedensohler, A., Decesari, S., Mircea, M., Facchini, M. C., Junninen, H., Kulmala, M., Lehtinen, K. E. J., and Laaksonen, A.: A comparison of new particle formation events in the

1194 boundary layer at three different sites in Europe, Boreal Environment Research, 14, 481-498,
1195 2009.

1196 Jones, A. M., and Harrison, R. M.: The effects of meteorological factors on atmospheric
1197 bioaerosol concentrations - a review, Sci. Total Environ., 326, 151-180,
1198 10.1016/j.scitotenv.2003.11.021, 2004.

1199 Kang, E., Root, M. J., Toohey, D. W., and Brune, W. H.: Introducing the concept of Potential
1200 Aerosol Mass (PAM), Atmospheric Chemistry and Physics, 7, 5727-5744, 2007.

1201 Karl, T., Potosnak, M., Guenther, A., Clark, D., Walker, J., Herrick, J. D., and Geron, C.:
1202 Exchange processes of volatile organic compounds above a tropical rain forest: Implications for
1203 modeling tropospheric chemistry above dense vegetation, J. Geophys. Res-Atmos, 109,
1204 10.1029/2004jd004738, 2004.

1205 Karl, T., Hansel, A., Cappellin, L., Kaser, L., Herdlinger-Blatt, I., and Jud, W.: Selective
1206 measurements of isoprene and 2-methyl-3-buten-2-ol based on NO+ ionization mass
1207 spectrometry, Atmos. Chem. Phys., 12, 11877-11884, 10.5194/acp-12-11877-2012, 2012.

1208 Karl, T., Kaser, L., and Turnipseed, A.: Eddy covariance measurements of isoprene and 232-
1209 MBO based on NO+ time-of-flight mass spectrometry, submitted to International Journal of
1210 Mass Spectrometry, 2013.

1211 Kaser, L., Karl, T., Schnitzhofer, R., Graus, M., Herdlinger-Blatt, I. S., DiGangi, J. P., Sive, B.,
1212 Turnipseed, A., Hornbrook, R. S., Zheng, W., Flocke, F. M., Guenther, A., Keutsch, F. N., Apel,
1213 E., and Hansel, A.: Comparison of different real time VOC measurement techniques in a
1214 ponderosa pine forest, Atmos. Chem. Phys., 13, 2893-2906, 10.5194/acp-13-2893-2013, 2013.

1215 Kaser, L., Karl, T., Guenther, A., Graus, M., Schnitzhofer, R., Turnipseed, A., Fischer, L.,
1216 Harley, P., Madronich, M., Gochis, D., Keutsch, E. N., and Hansel, A.: Undisturbed and
1217 disturbed above canopy ponderosa pine emissions: PTR-TOF-MS measurements and MEGAN
1218 2.1 model results, Atmospheric Chemistry and Physics, 13, 11935-11947, 10.5194/acp-13-
1219 11935-2013, 2013.

1220 Kleindienst, T. E., Jaoui, M., Lewandowski, M., Offenberg, J. H., Lewis, C. W., Bhave, P. V.,
1221 and Edney, E. O.: Estimates of the contributions of biogenic and anthropogenic hydrocarbons to
1222 secondary organic aerosol at a southeastern US location, Atmospheric Environment, 41, 8288-
1223 8300, 10.1016/j.atmosenv.2007.06.045, 2007.

1224 Kim, S., Karl, T., Guenther, A., Tyndall, G., Orlando, J., Harley, P., Rasmussen, R., and Apel,
1225 E.: Emissions and ambient distributions of Biogenic Volatile Organic Compounds (BVOC) in a
1226 ponderosa pine ecosystem: interpretation of PTR-MS mass spectra, Atmos. Chem. Phys., 10,
1227 1759-1771, 2010.

Kim, S., Wolfe, G. M., Mauldin, L., Cantrell, C., Guenther, A., Karl, T., Turnipseed, A., Greenberg, J., Hall, S. R., Ullmann, K., Apel, E., Hornbrook, R., Kajii, Y., Nakashima, Y., Keutsch, F. N., DiGangi, J. P., Henry, S. B., Kaser, L., Schnitzhofer, R., Graus, M., Hansel, A., Zheng, W., and Flocke, F. F.: Evaluation of HO_x sources and cycling using measurement-constrained model calculations in a 2-methyl-3-butene-2-ol (MBO) and monoterpene (MT) dominated ecosystem, Atmos. Chem. Phys., 13, 2031-2044, 10.5194/acp-13-2031-2013, 2013.

Kirkby, J., Curtius, J., Almeida, J., Dunne, E., Duplissy, J., Ehrhart, S., Franchin, A., Gagne, S., Ickes, L., Kurten, A., Kupc, A., Metzger, A., Riccobono, F., Rondo, L., Schobesberger, S., Tsagkogeorgas, G., Wimmer, D., Amorim, A., Bianchi, F., Breitenlechner, M., David, A., Dommen, J., Downard, A., Ehn, M., Flagan, R. C., Haider, S., Hansel, A., Hauser, D., Jud, W., Junninen, H., Kreissl, F., Kvashin, A., Laaksonen, A., Lehtipalo, K., Lima, J., Lovejoy, E. R., Makhmutov, V., Mathot, S., Mikkila, J., Minginette, P., Mogo, S., Nieminen, T., Onnela, A., Pereira, P., Petaja, T., Schnitzhofer, R., Seinfeld, J. H., Sipila, M., Stozhkov, Y., Stratmann, F., Tome, A., Vanhanen, J., Viisanen, Y., Vrtala, A., Wagner, P. E., Walther, H., Weingartner, E., Wex, H., Winkler, P. M., Carslaw, K. S., Worsnop, D. R., Baltensperger, U., and Kulmala, M.: Role of sulphuric acid, ammonia and galactic cosmic rays in atmospheric aerosol nucleation, Nature, 476, 429-U477, 10.1038/nature10343, 2011.

Kleindienst, T. E., Jaoui, M., Lewandowski, M., Offenberg, J. H., Lewis, C. W., Bhave, P. V., and Edney, E. O.: Estimates of the contributions of biogenic and anthropogenic hydrocarbons to secondary organic aerosol at a southeastern US location, Atmospheric Environment, 41, 8288-8300, 10.1016/j.atmosenv.2007.06.045, 2007.

Korhonen, H., Lehtinen, K. E. J., and Kulmala, M.: Multicomponent aerosol dynamics model UHMA: model development and validation, Atmospheric Chemistry and Physics, 4, 757-771, 2004.

Kulmala, M., Riipinen, I., Sipila, M., Manninen, H. E., Petaja, T., Junninen, H., Dal Maso, M., Mordas, G., Mirme, A., Vana, M., Hirsikko, A., Laakso, L., Harrison, R. M., Hanson, I., Leung, C., Lehtinen, K. E. J., and Kerminen, V. M.: Toward direct measurement of atmospheric nucleation, Science, 318, 89-92, 10.1126/science.1144124, 2007.

Kurpius, M. R., and Goldstein, A. H.: Gas-phase chemistry dominates O-3 loss to a forest, implying a source of aerosols and hydroxyl radicals to the atmosphere, Geophysical Research Letters, 30, 4, 10.1029/2002gl016785, 2003.

Lelieveld, J., Butler, T. M., Crowley, J. N., Dillon, T. J., Fischer, H., Ganzeveld, L., Harder, H., Lawrence, M. G., Martinez, M., Taraborrelli, D., and Williams, J.: Atmospheric oxidation capacity sustained by a tropical forest, Nature, 452, 737-740, 10.1038/nature06870, 2008.

Levin, E. J. T., Prenni, A. J., Petters, M. D., Kreidenweis, S. M., Sullivan, R. C., Atwood, S. A., Ortega, J., DeMott, P. J., and Smith, J. N.: An annual cycle of size-resolved aerosol

hygroscopicity at a forested site in Colorado, J. Geophys. Res-Atmos., 117, 10.1029/2011jd016854, 2012.

Levin, E. J. T., Prenni, A. J., Palm, B., Day, D., Campuzano-Jost, P., Winkler, P. M., Kreidenweis, S. M., DeMott, P. J., Jimenez, J., Smith, J. N.: Size-resolved aerosol composition and link to hygroscopicity at a forested site in Colorado, Atmospheric Chemistry and Physics, 14, 2657-2667, 10.5194/acp-14-2657-2014, 2014.

Lewandowski, M., Piletic, I. R., Kleindienst, T. E., Offenberg, J. H., Beaver, M. R., Jaoui, M., Docherty, K. S., and Edney, E. O.: Secondary organic aerosol characterisation at field sites across the United States during the spring-summer period, International Journal of Environmental Analytical Chemistry, 93, 1084-1103, 10.1080/03067319.2013.803545, 2013.

Lewis, C. W., Klouda, G. A., and Ellenson, W. D.: Radiocarbon measurement of the biogenic contribution to summertime PM-2.5 ambient aerosol in Nashville, TN, Atmospheric Environment, 38, 6053-6061, 10.1016/j.atmosenv.2004.06.011, 2004.

Lezberg, A. L., Battaglia, M. A., Shepperd, W. D., and Schoettle, A. W.: Decades-old silvicultural treatments influence surface wildfire severity and post-fire nitrogen availability in a ponderosa pine forest, Forest Ecol. Manag., 255, 49-61, 10.1016/j.foreco.2007.08.019, 2008.

Linkhart, B. D., and Reynolds, R. T.: Lifetime reproduction of Flammulated Owls in Colorado, J. Raptor Res., 40, 29-37, 10.3356/0892-1016(2006)40[29:lrofoi]2.0.co;2, 2006.

Linkhart, B. D., and Reynolds, R. T.: Return rate, fidelity, and dispersal in a breeding population of flammulated owls (Otus flammeolus), Auk, 124, 264-275, 10.1642/0004-8038(2007)124[264:rrfadi]2.0.co;2, 2007.

Mahowald, N., Ward, D. S., Kloster, S., Flanner, M. G., Heald, C. L., Heavens, N. G., Hess, P. G., Lamarque, J. F., and Chuang, P. Y.: Aerosol Impacts on Climate and Biogeochemistry, Annual Review of Environment and Resources, Vol 36, 36, 45-74, 10.1146/annurev-environ-042009-094507, 2011.

Mao, J., Ren, X., Zhang, L., Van Duin, D. M., Cohen, R. C., Park, J. H., Goldstein, A. H., Paulot, F., Beaver, M. R., Crounse, J. D., Wennberg, P. O., DiGangi, J. P., Henry, S. B., Keutsch, F. N., Park, C., Schade, G. W., Wolfe, G. M., Thornton, J. A., and Brune, W. H.: Insights into hydroxyl measurements and atmospheric oxidation in a California forest, Atmospheric Chemistry and Physics, 12, 8009-8020, 10.5194/acp-12-8009-2012, 2012.

Massman, W. J., Frank, J. M., and Mooney, S. J.: ADVANCING INVESTIGATION AND PHYSICAL MODELING OF FIRST-ORDER FIRE EFFECTS ON SOILS, Fire Ecology, 6, 36-54, 10.4996/fireecology.0601036, 2010.

Matsui, H., M. Koike, Y. Kondo, N. Takegawa, A. Wiedensohler, J. D. Fast, and R. A. Zaveri, 2011: Impact of new particle formation on the concentrations of aerosols and cloud condensation nuclei around beijingBeijing. J. Geophys. Res-Atmos., 116, 19, DOI: 10.1029/2011jd016025, 2011.

Mauldin, R. L., Eisele, F. L., Cantrell, C. A., Kosciuch, E., Ridley, B. A., Lefer, B., Tanner, D. J., Nowak, J. B., Chen, G., Wang, L., and Davis, D.: Measurements of OH aboard the NASA P-3 during PEM-Tropics B, Journal of Geophysical Research-Atmospheres, 106, 32657-32666, 10.1029/2000jd900832, 2001.

Mirme, S., Mirme, A., Minikin, A., Petzold, A., Horrak, U., Kerminen, V. M., and Kulmala, M.: Atmospheric sub-3 nm particles at high altitudes, Atmos. Chem. Phys., 10, 437-451, 2010.

Morris, C. E., Conen, F., Hufffman, J. A., Phillips, V., Pöschl, U. and Sands, D. C.: Bioprecipitation: A feedback cycle linking Earth history, ecosystem dynamics and land use through biological ice nucleators in the atmosphere, Global Change Biology, Accepted, 2013.

Moteki, N., Kondo, Y., Nakamura, S.: Method to measure refractive indices of small nonspherical particles: Application to black carbon particles, J. Aerosol. Sci., 41, 5, 513–521, 2010.

Orlando, J. J., and Tyndall, G. S.: Laboratory studies of organic peroxy radical chemistry: an overview with emphasis on recent issues of atmospheric significance (vol 41, pg 6294, 2012), Chemical Society Reviews, 41, 8213-8213, 2012.

Ortega, A. M., Day, D. A., Cubison, M. J., Brune, W. H., Bon, D., de Gouw, J. A., Jimenez, J. L.: Secondary organic aerosol formation and primary organic aerosol oxidation from biomass burning smoke in a flow reactor during FLAME-3. Atmospheric Chemistry and Physics, 13, 11551-11571, 10.5194/acp-13-11551-2013, 2013.

Paasonen, P., Asmi, A., Petaja, T., Kajos, M. K., Aijala, M., Junninen, H., Holst, T., Abbatt, J. P. D., Arneth, A., Birmili, W., van der Gon, H. D., Hamed, A., Hoffer, A., Laakso, L., Laaksonen, A., Leaitch, W. R., Plass-Dulmer, C., Pryor, S. C., Raisanen, P., Swietlicki, E., Wiedensohler, A., Worsnop, D. R., Kerminen, V. M., and Kulmala, M.: Warming-induced increase in aerosol number concentration likely to moderate climate change, Nature Geoscience, 6, 438-442, 10.1038/ngeo1800, 2013.

Peeters, J., Nguyen, T. L., and Vereecken, L.: HOx radical regeneration in the oxidation of isoprene, Physical Chemistry Chemical Physics, 11, 5935-5939, 10.1039/b908511d, 2009.

Petters, M. D., and Kreidenweis, S. M.: A single parameter representation of hygroscopic growth and cloud condensation nucleus activity, Atmos. Chem. Phys., 7, 1961-1971, 2007.

1330 Pöhlker, C., Wiedemann, K. T., Sinha, B., Shiraiwa, M., Gunthe, S. S., Smith, M., Su, H.,
1331 Artaxo, P., Chen, Q., Cheng, Y. F., Elbert, W., Gilles, M. K., Kilcoyne, A. L. D., Moffet, R. C.,
1332 Weigand, M., Martin, S. T., Poeschl, U., and Andreae, M. O.: Biogenic Potassium Salt Particles
1333 as Seeds for Secondary Organic Aerosol in the Amazon, Science, 337, 1075-1078,
1334 10.1126/science.1223264, 2012.

1335 Pöschl, U., Martin, S. T., Sinha, B., Chen, Q., Gunthe, S. S., Huffman, J. A., Borrmann, S.,
1336 Farmer, D. K., Garland, R. M., Helas, G., Jimenez, J. L., King, S. M., Manzi, A., Mikhailov, E.,
1337 Pauliquevis, T., Petters, M. D., Prenni, A. J., Roldin, P., Rose, D., Schneider, J., Su, H., Zorn, S.
1338 R., Artaxo, P., and Andreae, M. O.: Rainforest Aerosols as Biogenic Nuclei of Clouds and
1339 Precipitation in the Amazon, Science, 329, 1513-1516, 10.1126/science.1191056, 2010.

1340 Prenni, A. J., Tobo, Y., Garcia, E., DeMott, P. J., Huffman, J. A., McCluskey, C. S.,
1341 Kreidenweis, S. M., Prenni, J. E., Pohlker, C., and Poschl, U.: The impact of rain on ice nuclei
1342 populations at a forested site in Colorado, Geophys. Res. Lett., 40, 227-231,
1343 10.1029/2012gl053953, 2013.

1344 Pryor, S.C., Barthelmie, R. J., and Hornsby, K. E.: Size-resolved particle fluxes and vertical
1345 gradients over and in a sparse pine forest. Aerosol Sci. and Tech., 47, 1248-1257, 2013.

1346 Pryor, S. C., Spaulding, A. M., and Barthelmie, R. J.: New particle formation in the Midwestern
1347 USA: Event characteristics, meteorological context and vertical profiles, Atmospheric
1348 Environment, 44, 4413-4425, 10.1016/j.atmosenv.2010.07.045, 2010.

1349 Rhoades, C. C., Battaglia, M. A., Rocca, M. E., and Ryan, M. G.: Short- and medium-term
1350 effects of fuel reduction mulch treatments on soil nitrogen availability in Colorado conifer
1351 forests, Forest Ecol. Manag., 276, 231-238, 10.1016/j.foreco.2012.03.028, 2012.

1352 Robinson, N. H., Allan, J. D., Huffman, J. A., Kaye, P. H., Foot, V. E., and Gallagher, M.:
1353 Cluster analysis of WIBS single-particle bioaerosol data, Atmospheric Measurement Techniques,
1354 6, 337-347, 10.5194/amt-6-337-2013, 2013.

1355 Rogers, D. C., DeMott, P. J., Kreidenweis, S. M., and Chen, Y. L.: A continuous-flow diffusion
1356 chamber for airborne measurements of ice nuclei, Journal of Atmospheric and Oceanic
1357 Technology, 18, 725-741, 10.1175/1520-0426(2001)018<0725:acfdcf>2.0.co;2, 2001.

1358 Rollins, A. W., Smith, J. D., Wilson, K. R., and Cohen, R. C.: Real Time In Situ Detection of
1359 Organic Nitrates in Atmospheric Aerosols, Environmental Science & Technology, 44, 5540-
1360 5545, 10.1021/es100926x, 2010.

1361
1362 Schobesberger, S., Vaananen, R., Leino, K., Virkkula, A., Backman, J., Pohja, T., Siivola, E.,
1363 Franchin, A., Mikkila, J., Paramonov, M., Aalto, P. P., Krejci, R., Petaja, T., and Kulmala, M.:

1364 Airborne measurements over the boreal forest of southern Finland during new particle formation
1365 events in 2009 and 2010, Boreal Environ. Res., 18, 145-163, 2013.

1366 Schumacher, C. J., Pöhlker, C., Aalto, P., Hiltunen, V., Petäjä, T., Kulmala, M., Pöschl, U., and
1367 Huffman, J. A.: Seasonal cycles of fluorescent biological aerosol particles in boreal and semi-
1368 arid forests of Finland and Colorado. Atmospheric Chemistry and Physics, 13, 11987-12001,
1369 10.5194/acp-13-11987-2013, 2013.

1370 Shrivastava, M., Fast, J., Easter, R., Gustafson, W. I., Zaveri, R. A., Jimenez, J. L., Saide, P., and
1371 Hodzic, A.: Modeling organic aerosols in a megacity: comparison of simple and complex
1372 representations of the volatility basis set approach, Atmospheric Chemistry and Physics, 11,
1373 6639-6662, 10.5194/acp-11-6639-2011, 2011.

1374 Smith, J. N., Moore, K. F., McMurry, P. H., and Eisele, F. L.: Atmospheric measurements of
1375 sub-20 nm diameter particle chemical composition by thermal desorption chemical ionization
1376 mass spectrometry, Aerosol Science and Technology, 38, 100-110,
1377 10.1080/02786820490249036, 2004.
1378
1379 Soil Conservation Service: Soil Survey of Pike National Forest, Eastern Part, Colorado, Parts of
1380 Douglas, El Paso, Jefferson and Teller Counties. United States Department of Agriculture,
1381 Forest Service and Soil Conservation Service. 106 pages, 1992.
1382
1383 Stone, D., Whalley, L. K., and Heard, D. E.: Tropospheric OH and HO2 radicals: field
1384 measurements and model comparisons, Chemical Society Reviews, 41, 6348-6404,
1385 10.1039/c2cs35140d, 2012.

1386 Tanner, D. J., Jefferson, A., and Eisele, F. L.: Selected ion chemical ionization mass
1387 spectrometric measurement of OH, Journal of Geophysical Research-Atmospheres, 102, 6415-
1388 6425, 10.1029/96jd03919, 1997.
1389
1390 Thornton, J. A., Wooldridge, P. J., Cohen, R. C., Martinez, M., Harder, H., Brune, W. H.,
1391 Williams, E. J., Roberts, J. M., Fehsenfeld, F. C., Hall, S. R., Shetter, R. E., Wert, B. P., and
1392 Fried, A.: Ozone production rates as a function of NOx abundances and HOx production rates in
1393 the Nashville urban plume, J. Geophys. Res., 107, 4146-4163, 10.1029/2001JD000932, 2002.

1394 Tobo, Y., Prenni, A.J., DeMott, P.J., Huffman, J.A., McCluskey, C.S., Tian, G., Pöhlker, C.,
1395 Pöschl, U., Kreidenweis, S.M.: Biological aerosol particles as a key determinant of ice nuclei
1396 populations in a forest ecosystem. J. Geophys. Res-Atmos., 118, 10100-10110,
1397 doi:10.1002/jgrd.50801, 2013.

1398 Vogel, A. L., Aijala, M., Bruggemann, M., Ehn, M., Junninen, H., Petaja, T., Worsnop, D. R.,
1399 Kulmala, M., Williams, J., and Hoffmann, T.: Online atmospheric pressure chemical ionization
1400 ion trap mass spectrometry (APCI-IT-MSn) for measuring organic acids concentrated bulk

aerosol - a laboratory and field study, Atmospheric Measurement Techniques, 6, 431-443, 10.5194/amt-6-431-2013, 2013.

Vorosmarty, C. J., McIntyre, P. B., Gessner, M. O., Dudgeon, D., Prusevich, A., Green, P., Glidden, S., Bunn, S. E., Sullivan, C. A., Liermann, C. R., and Davies, P. M.: Global threats to human water security and river biodiversity, Nature, 467, 555-561, 10.1038/nature09440, 2010.

Wagner, N. L., Dubé, W. P., Washenfelder, R. A., Young, C. J., Pollack, I. B., Ryerson, T. B., and Brown, S. S.: Diode laser-based cavity ring-down instrument for NO3, N2O5, NO, NO2 and O3 from aircraft, Atmos. Meas. Tech., 4, 1227-1240, 2011.Williams, B. J., Jayne, J. T., Lambe, A. T., Hohaus, T., Kimmel, J. R., Sueper, D., Brooks, W., Williams,.L. R., Trimborn, A. M., Martinez, R. E., Hayes,.P. L., Jimenez, J. L., Kreisberg, N. M., Hering, S. V., Worton, D. R., Goldstein, A. H., Worsnop, D. R.: The First Combined Thermal Desorption Aerosol Gas Chromatograph – Aerosol Mass Spectrometer (TAG-AMS), Aerosol Science and Technology, 48, 4, 358370, DOI:10.1080/02786826.2013.875114, 2014.

Wolfe, G. M., Thornton, J. A., Bouvier-Brown, N. C., Goldstein, A. H., Park, J. H., McKay, M., Matross, D. M., Mao, J., Brune, W. H., LaFranchi, B. W., Browne, E. C., Min, K. E., Wooldridge, P. J., Cohen, R. C., Crounse, J. D., Faloona, I. C., Gilman, J. B., Kuster, W. C., de Gouw, J. A., Huisman, A., and Keutsch, F. N.: The Chemistry of Atmosphere-Forest Exchange (CAFE) Model - Part 2: Application to BEARPEX-2007 observations, Atmospheric Chemistry and Physics, 11, 1269-1294, 10.5194/acp-11-1269-2011, 2011.

Wolfe, G. M., Cantrell, C., Kim, S., Mauldin III, R. L., Karl, T., Harley, P., Turnipseed, A., Zheng, W., Flocke, F., Apel, E. C., Hornbrook, R. S., Hall, S. R., Ullmann, K., Henry, S. B., DiGangi, J. P., Boyle, E. S., Kaser, L., Schnitzhofer, R., Hansel, A., Graus, M., Nakashima, Y., Kajii, Y., Guenther, A., Keutsch, R. N.: Missing peroxy radical sources within a rural forest canopy, Atmospheric Chemistry and Physics Discussions, 13, 31713-31759, 10.5194/acp-13-31713-2013, 2013.

Yatavelli, R. L. N., Lopez-Hilfiker, F., Wargo, J. D., Kimmel, J. R., Cubison, M. J., Bertram, T. H., Jimenez, J. L., Gonin, M., Worsnop, D. R., and Thornton, J. A.: A Chemical Ionization High-Resolution Time-of-Flight Mass Spectrometer Coupled to a Micro Orifice Volatilization Impactor (MOVI-HRToF-CIMS) for Analysis of Gas and Particle-Phase Organic Species, Aerosol Science and Technology, 46, 1313-1327, 10.1080/02786826.2012.712236, 2012.

Yatavelli, R. L. N., Stark, H., Thompson, S. L., Kimmel, J. R., Cubison, M. J., Day, D. A., Campuzano-Jost, P., Palm, B. B., Hodzic, A., Thornton, J. A., Jayne, J. T., Worsnop, D. R., and Jimenez, J. L.: Semicontinuous measurements of gas-particle partitioning of organic acids in a ponderosa pine forest using a MOVI-HRToF-CIMS, Atmospheric Chemistry and Physics, 14, 1527-1546, 10.5194/acp-14-1527-2014, 2014.

Zhang, H. F., Worton, D. R., Lewandowski, M., Ortega, J., Rubitschun, C. L., Park, J. H., Kristensen, K., Campuzano-Jost, P., Day, D. A., Jimenez, J. L., Jaoui, M., Offenberg, J. H., Kleindienst, T. E., Gilman, J., Kuster, W. C., de Gouw, J., Park, C., Schade, G. W., Frossard, A.

A., Russell, L., Kaser, L., Jud, W., Hansel, A., Cappellin, L., Karl, T., Glasius, M., Guenther, A., Goldstein, A. H., Seinfeld, J. H., Gold, A., Kamens, R. M., and Surratt, J. D.: Organosulfates as Tracers for Secondary Organic Aerosol (SOA) Formation from 2-Methyl-3-Buten-2-ol (MBO) in the Atmosphere, Environ. Sci. Technol., 46, 9437-9446, 10.1021/es301648z, 2012.

Zhao, J., Eisele, F. L., Titcombe, M., Kuang, C. G., and McMurry, P. H.: Chemical ionization mass spectrometric measurements of atmospheric neutral clusters using the cluster-CIMS, J. Geophys. Res-Atmos., 115, 19, 10.1029/2009jd012606, 2010.

Zhao, J., Smith, J. N., Eisele, F. L., Chen, M., Kuang, C., and McMurry, P. H.: Observation of neutral sulfuric acid-amine containing clusters in laboratory and ambient measurements, Atmos. Chem. Phys., 11, 10823-10836, 10.5194/acp-11-10823-2011, 2011.

Zhao, Y. L., Kreisberg, N. M., Worton, D. R., Teng, A. P., Hering, S. V., and Goldstein, A. H.: Development of an In Situ Thermal Desorption Gas Chromatography Instrument for Quantifying Atmospheric Semi-Volatile Organic Compounds, Aerosol Science and Technology, 47, 258-266, 10.1080/02786826.2012.747673, 2013.

Figure 1: Manitou Experimental Forest Observatory (MEFO). A. Map showing general area within Colorado and its relationship to neighboring states. B. Site location relative to the Front Range urban corridor including Denver and Colorado Springs. C. Close-up aerial photograph showing the open-canopy ponderosa pine-dominated forest with the (i) micrometeorological tower, (ii) chemistry tower, and (iii) water manipulation experiment. D. Close up picture of the chemistry tower. E. Close of up picture of micrometeorological tower. The two towers shown in C are approximately 300 m apart. Maps in panels A and B were produced using ArcGIS software (ESRI Inc., Redlands, CA).

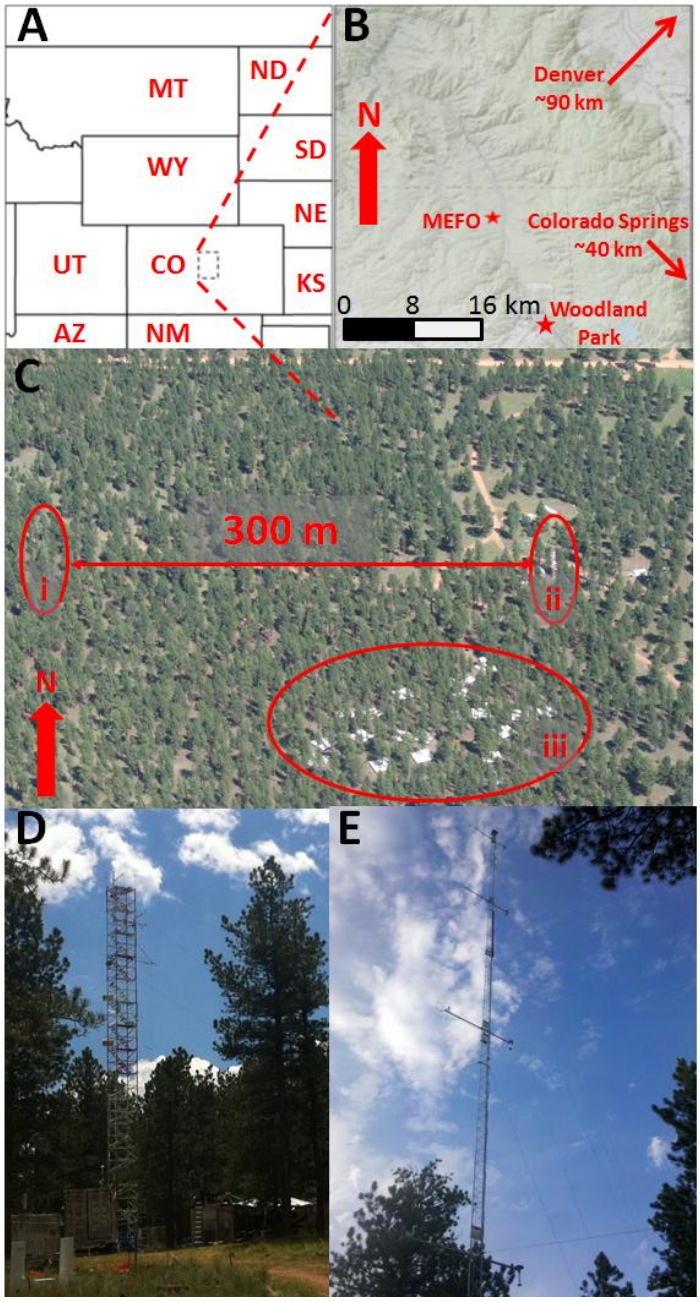

Figure 2: Average diel net radiation (downwelling minus upwelling), latent heat flux, sensible heat flux and net CO_2 flux for four representative months. All properties were measured from 28 m at the top of the chemistry tower in 2011. Each data point represents a 30 minute average for that time period. The y-axis limits are the same for each plot except for January, where the scale is ½ of the other three months. The shaded area for net radiation and error bars for CO_2 flux represent ± 1 standard deviation. Error bars for sensible and latent heat fluxes have been omitted for clarity.

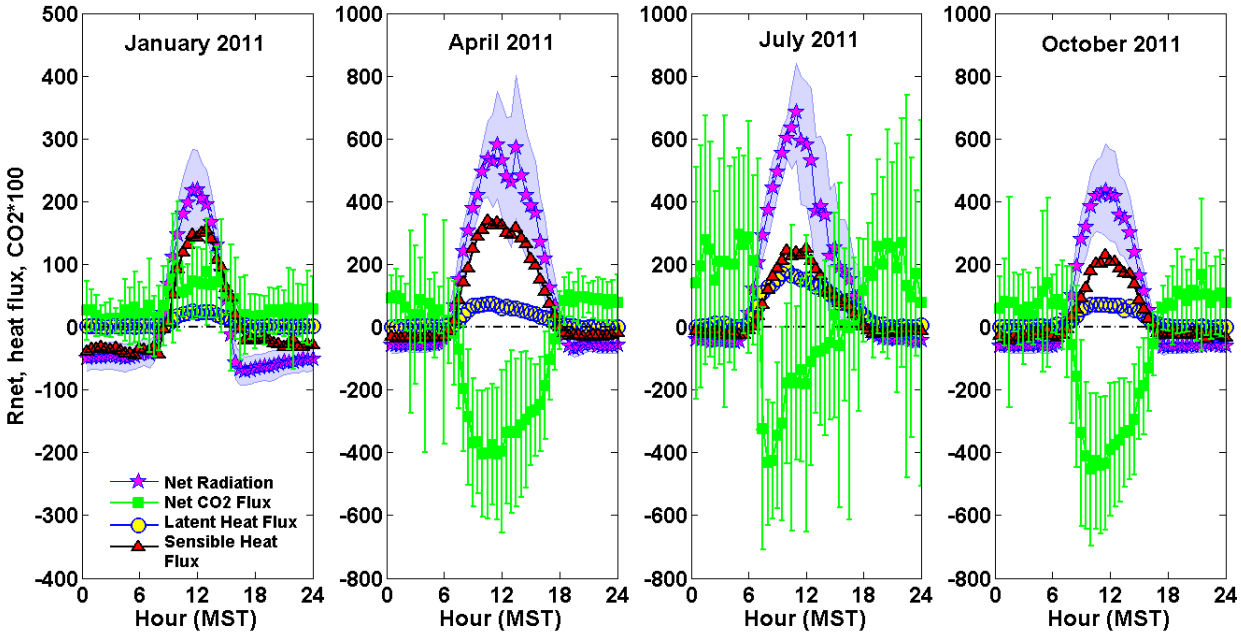

Figure 3: Wind direction distributions (5-minute averages binned every 10 degrees) from the MEFO chemistry tower. Panels a, c and e are Daytime wind distributions (9:00-17:00 MST) whereas panels b, d and f are for Nighttime hours (20:00 until 5:00, MST). Summer includes data from June-August 2010. Winter includes data from December 2010 to February 2011. Measurement height is noted on the panels.

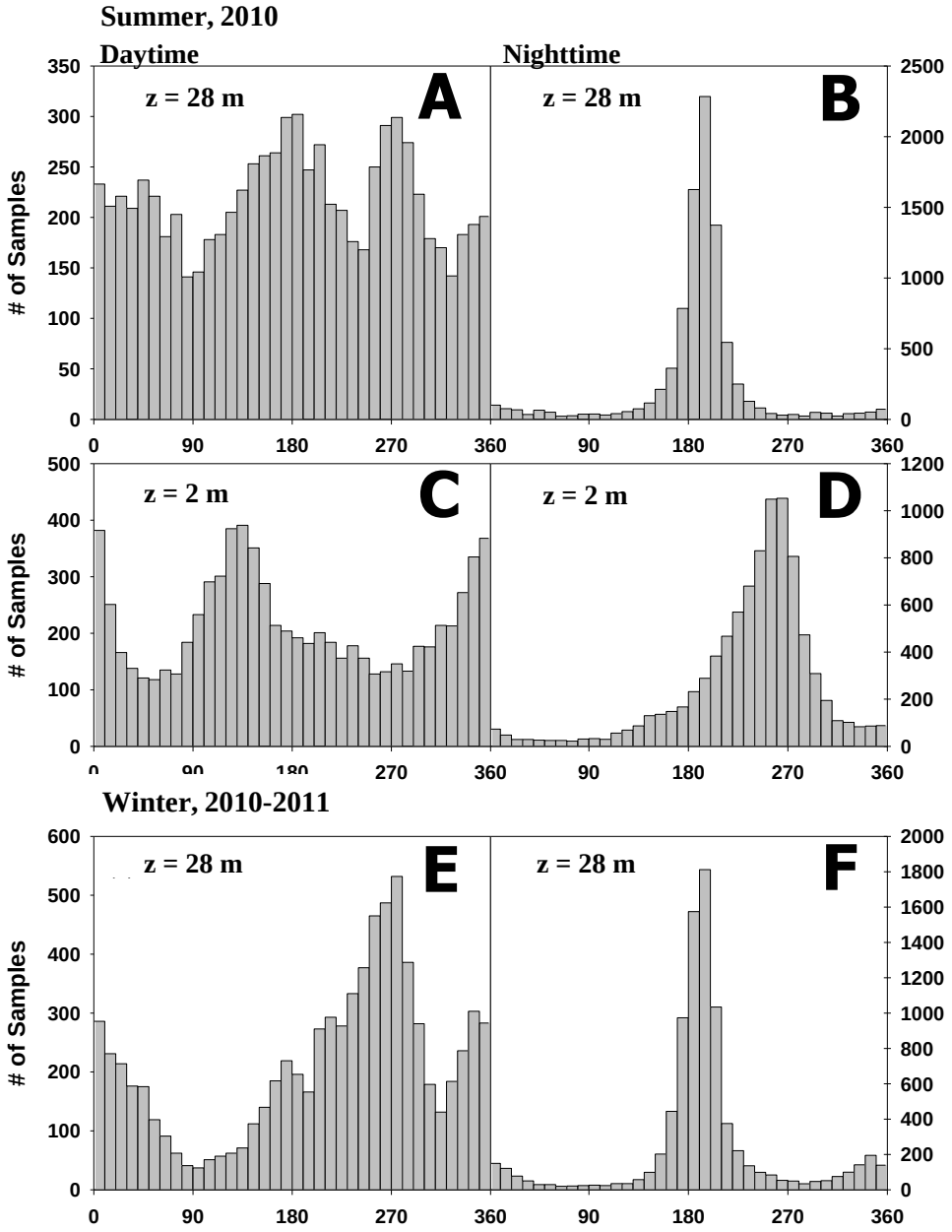

Figure 4: Hydrological measurement summary at the Manitou Experimental Forest Observatory. Annual accumulated precipitation from rain and snow (A), soil moisture at 3 depths (B), and soil temperature at three different depths (C). Panel A includes data from hydrological years 2010-2013 whereas panels B and C include data from 2010-2012.

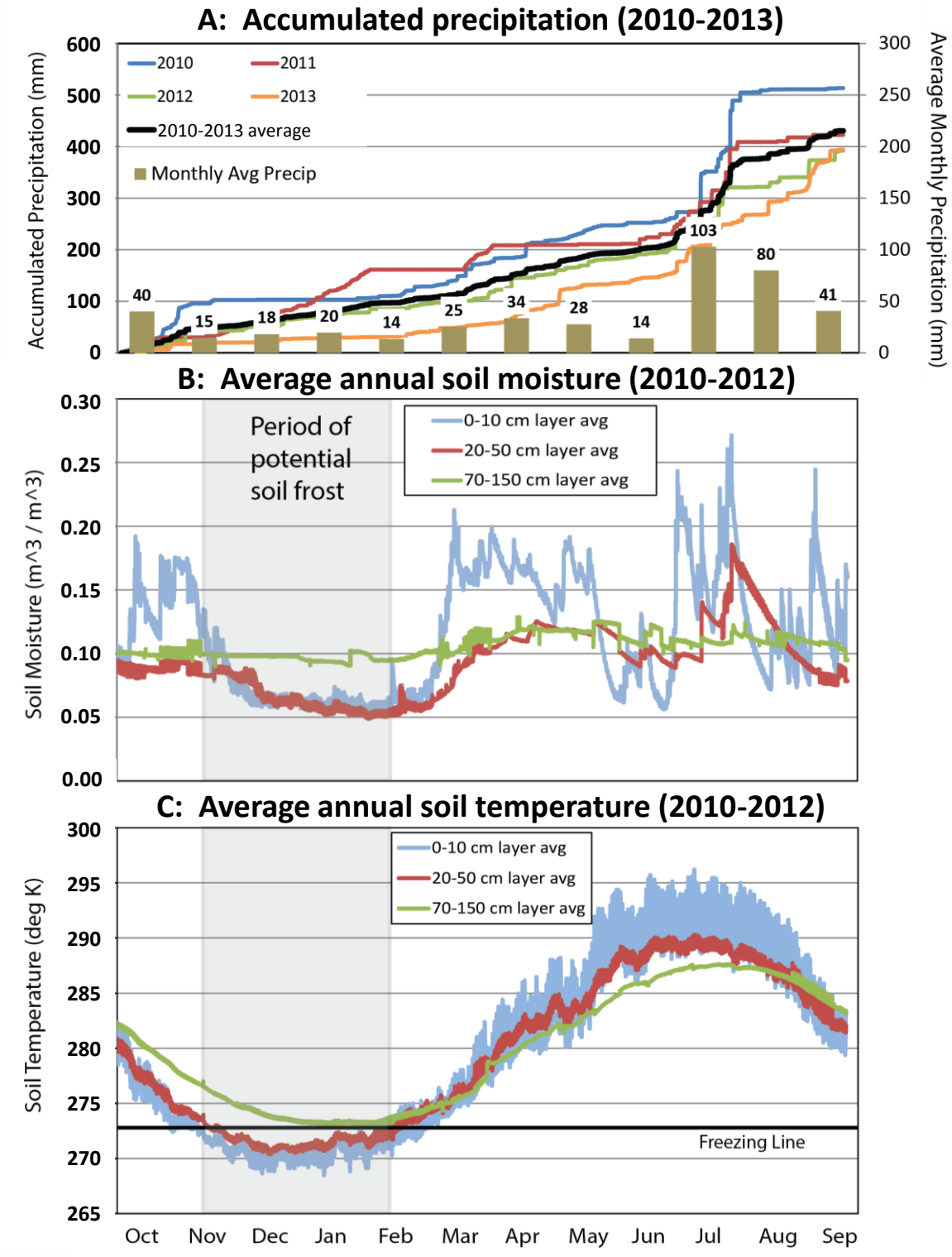

Figure 5: Average daytime and nighttime vertical fluxes of monoterpenes ($C_{10}H_{16}$) and 2-methyl-3-buten-2-ol (232MBO, $C_5H_{10}O$) during August 2010. The average daytime integrated flux ratio of MBO:Monoterpenes is 1.65. Fluxes within ± 0.1 mg m^{-2} hr^{-1} m^{-1} are shown within the shaded grey area to indicate the detection limit. Error bars indicate the standard deviation of all measurements for that period and chemical species.

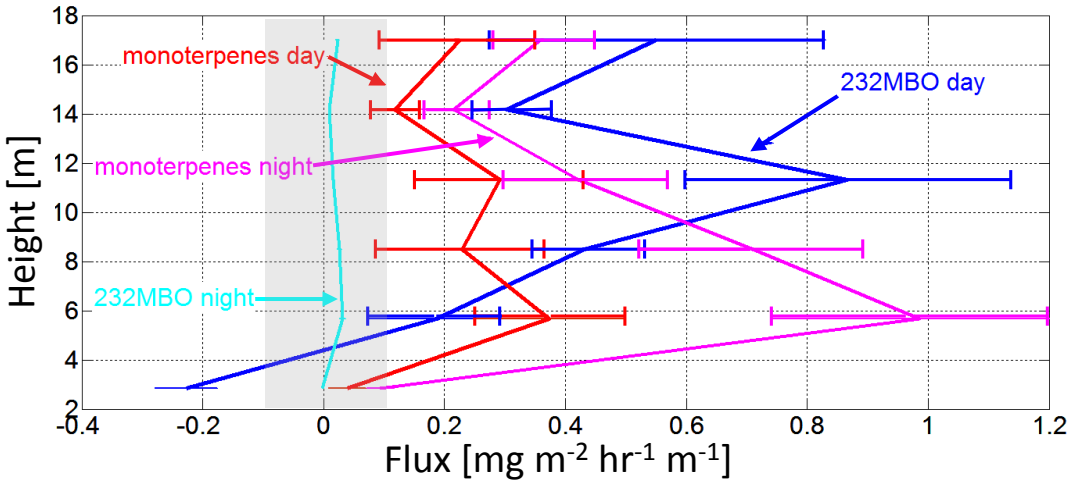

Figure 6: 6A (adapted from Kaser et al., 2013b) shows the sum of MT and MBO+isoprene measurements as reported by the PTR-TOF-MS from 25.1 m on the chemistry tower from August 4 (DOY = 216) to August 11, 2010 (DOY=223). A-1 shows the above-canopy fluxes, while A-2 shows the corresponding concentrations in ppbv. 6B shows diurnal profiles of (B-1) isoprene, (B-2) toluene, (B-3) MBO, and (B-4) sum of monoterpenes during all of August 2010 as measured using TOGA. Box boundaries indicate inter-quartile range, median is indicated as the line through the box, and whisker lengths indicate the total measurement range.

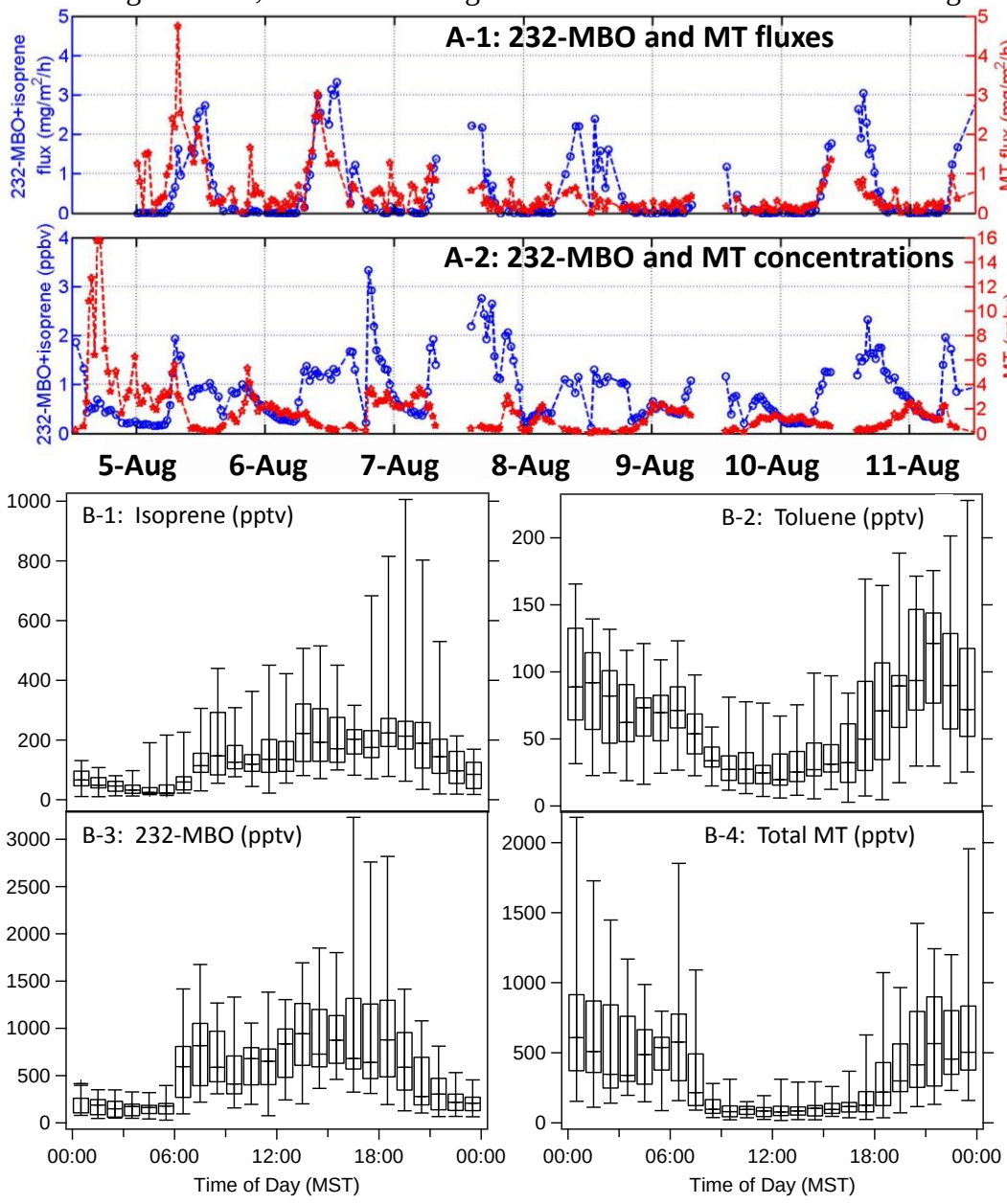

Figure 7: Average modeled and measured diurnal cycles of (a) within-canopy peroxy radical mixing ratios, and (b) above-canopy formaldehyde fluxes. The measured and modeled results for both compounds include the hourly averages from the August 2010 BEACHON ROCS intensive measurement campaign. Model calculations of HCHO fluxes and peroxy radicals are described in DiGangi et al. (2011) and Wolfe et al. (2013), respectively.

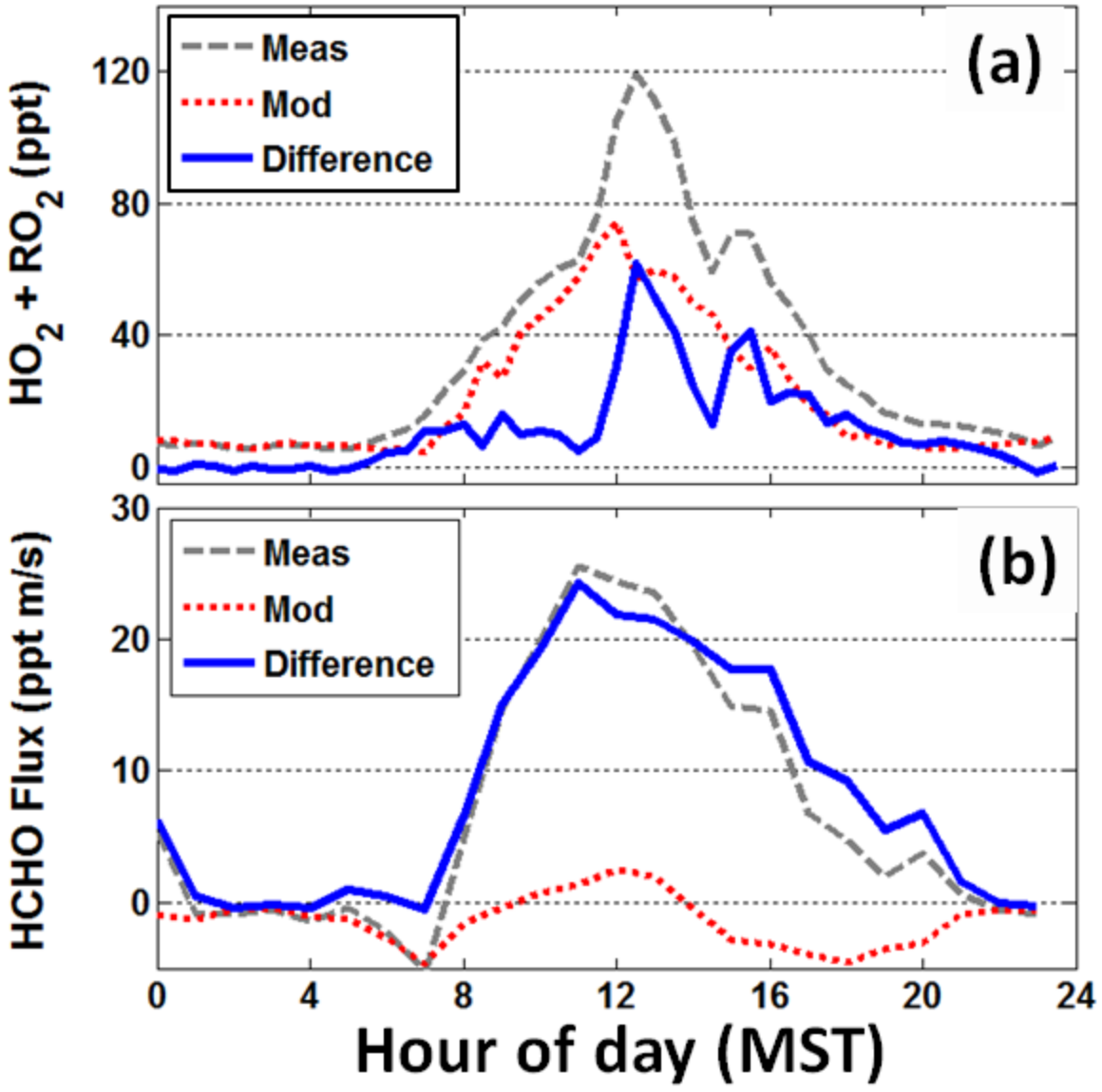

Figure 8: Examination of RO_2 fate and its relation to anthropogenic influence on 24 August 2010 during BEACHON-ROCS. The first panel (A) shows median concentrations of NO, NO_2, HO_2 , and HO_2 +RO_2 over the course of this day. Wind speed and direction (C) show the wind shifting from out of the south to out of the southeast just prior to noon indicating an anthropogenic-influence from the Colorado Springs area. This transition is also reflected in the NO increase in panel A. The middle panel (B) shows the calculated RO_2 loss percentage from reaction with NO or HO_2 based on measured NO and HO_2 concentrations and on rate constants obtained from the IUPAC database. Each symbol in B represents the median value from thirty minute time bins. Figure adapted from DiGangi et al. (2012).

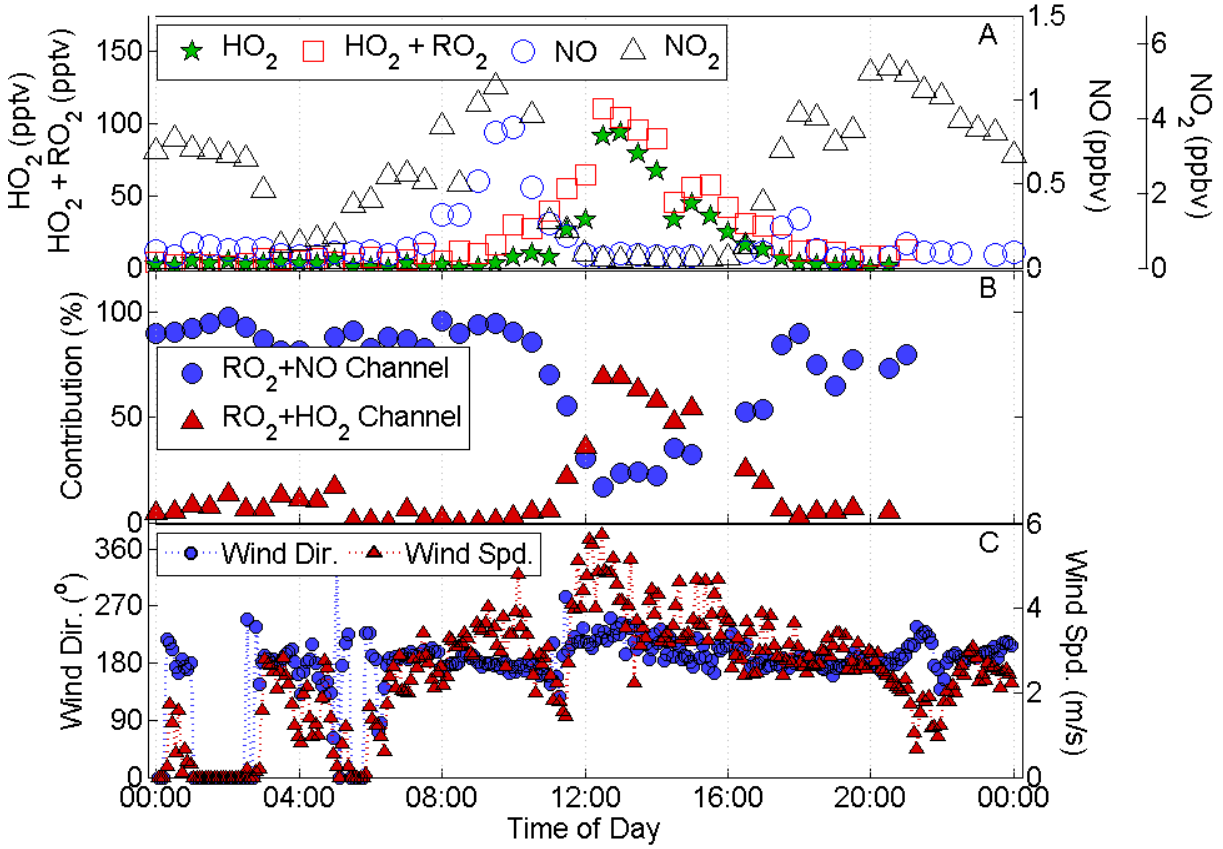

Figure 9: Three representative days of particle size distributions (a), wind speed, wind direction and sulfate aerosol mass (b) during July 27-29, 2011. In panel (a), the mobility diameter is on the y-axis, time is on the x-axis, and the color bar indicates particle number concentration (dN/dlogDp) in cm^{-3}. In panel (b), the sulfate aerosol mass is multiplied by 4 and is listed on the 2nd y-axis along with wind speed.

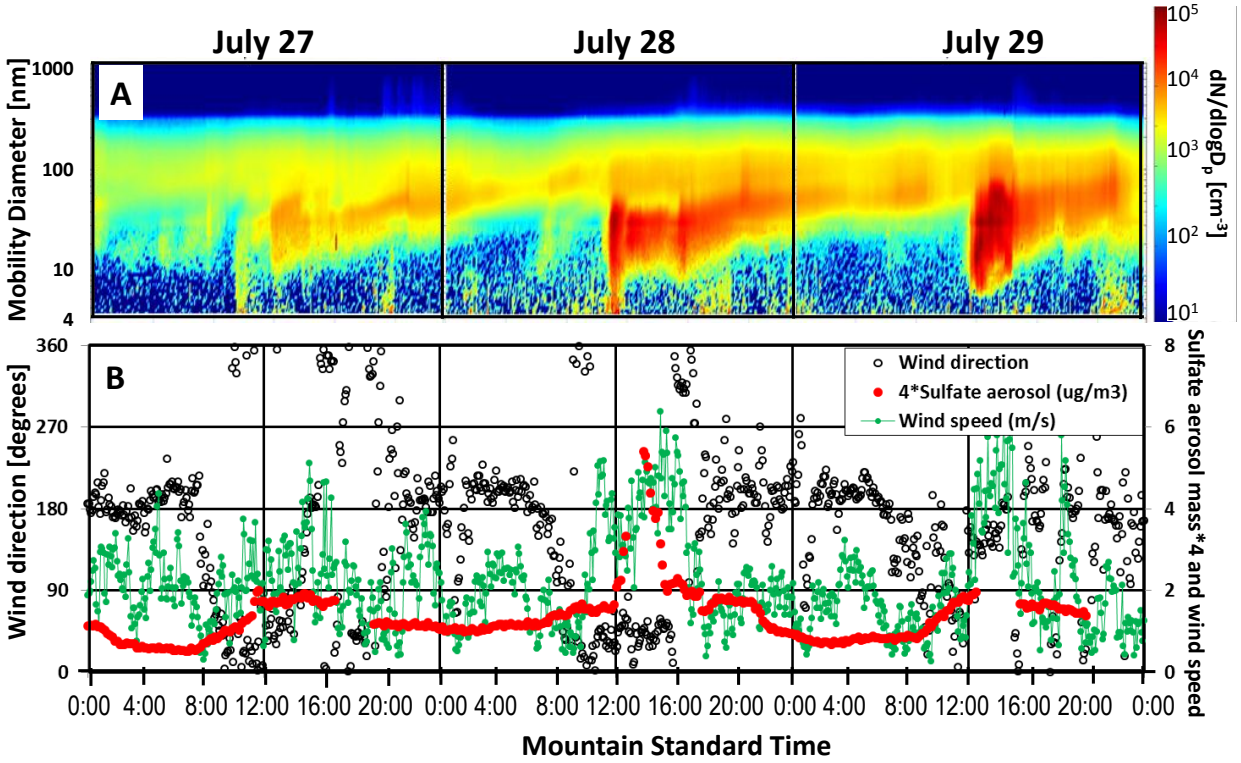

Figure 10: Aerosol mass spectrometer (AMS) and Single Particle Soot Photometer (SP2) results of bulk PM_1 aerosol composition during July and August 2011. Black carbon (BC) is measured by the SP2 and all others (organics, nitrate, sulfate, and ammonium) are from the AMS. Panel a) shows the time series of mass loadings, panel b) shows the average size-resolved aerosol distributions, and panel c) shows the diurnal trends of each of the individual species averaged over the study period. The box plot boundaries in c) represent the standard deviations, and the whisker lengths indicate the 25th and 75th percentiles of the measurements. The center line through each box indicates the median. Note that the majority of the aerosol is composed of organic species, and that in all panels, black carbon mass has been multiplied by 6 and the other (sulfate, nitrate, and ammonium) species' masses have been multiplied by 3. The diameters for the BC measurements are estimated using an assumed density of 1.8 g cm^{-3} as indicated in the text (Section 3.3).

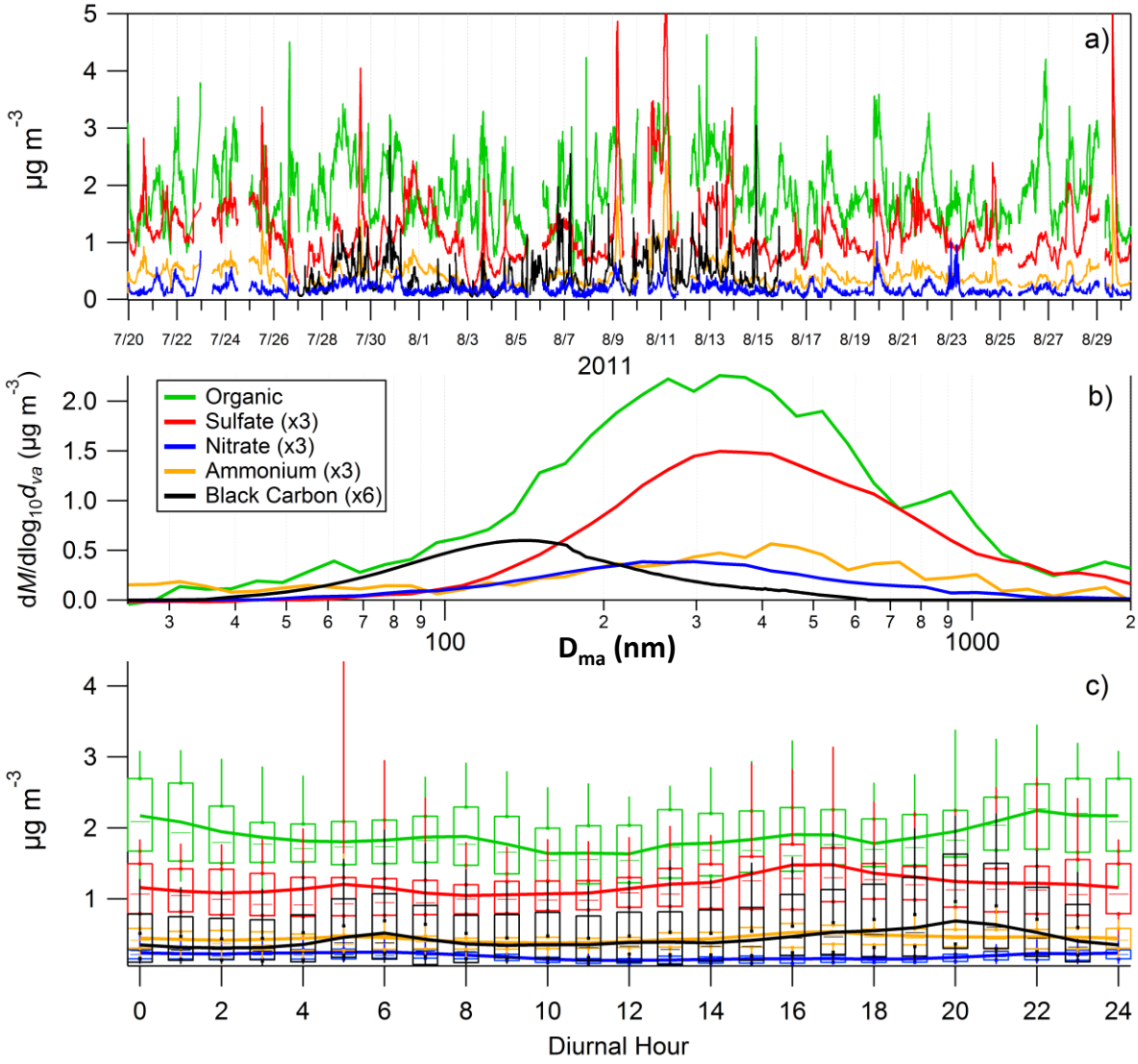

Figure 11: Residence Time Analysis (RTA) from WRF-Chem estimates the amount of time that air masses originate from the various locations in the region. These simulations estimate 48 hour back-trajectories at MEFO (July 27 to August 26, 2011). Three major Front Range cities (Denver, Colorado Springs, and Pueblo), are shown, and open circles indicate the cities' primary coal-fired power plants. The left panel indicates that the majority of the low NO_2 concentration results (0-50th percentile) are from air masses that originate from the west. The right panel shows that the highest 10% of NO_2 concentrations originate from the Front Range cities and are advected to the site.

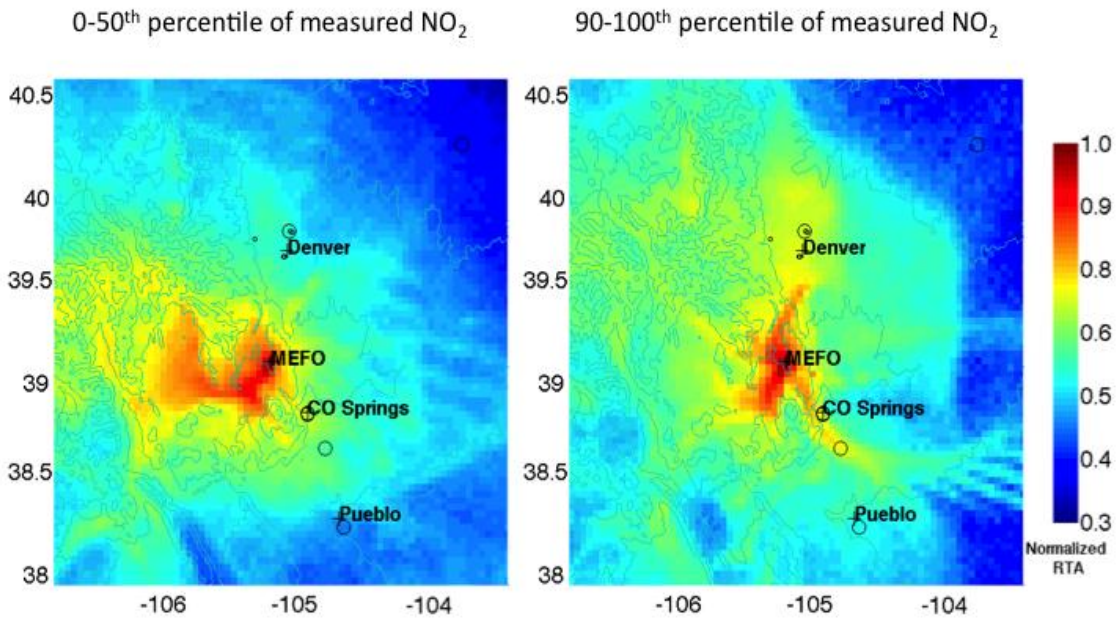

Figure 12: Modeled and measured average diurnal profiles of total organic aerosol (TOA) mass concentrations at MEFO during BEACHON-RoMBAS-2011. Aerosol mass spectrometry (AMS) observations are shown as black circles (with 1 σ variability shown in gray). Predicted TOA is indicated in yellow (with variability shown by the yellow bars). The predicted TOA is the sum of the contributions: primary OA (red), biogenic secondary organic aerosol (SOA) from OH and O_3 chemistry (green), biogenic SOA from NO_3 nighttime chemistry (purple) and anthropogenic SOA (yellow). Each plot (starting with green) is additive (equal to that process plus the sum of the processes below it): e.g. the purple plot shows the contributions from primary OA, biogenic SOA from OH and O_3 and biogenic SOA + NO_3. Biogenic SOA (both day and night) are the largest contributors to TOA, but anthropogenic species (gold) also make a significant contribution.

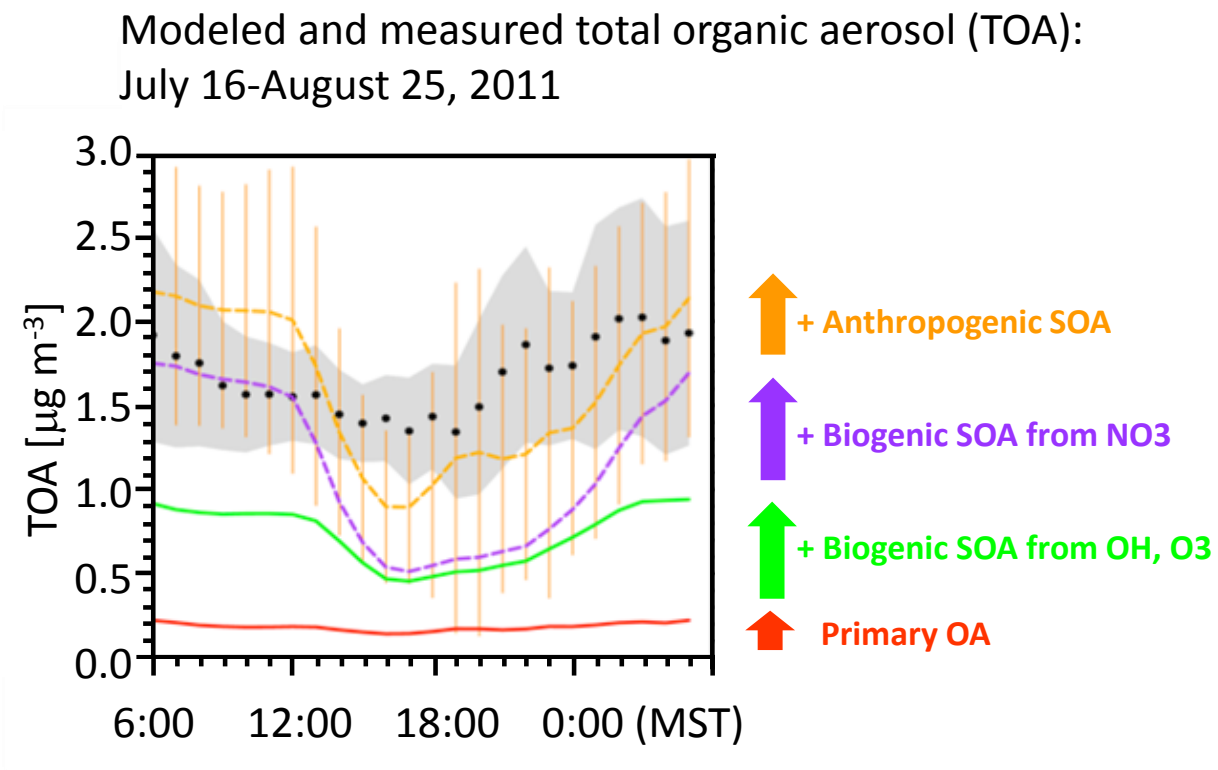

Figure 13: July 29, 2011 particle size distributions observed (a) and modeled with WRF-Chem (b). White areas in panel (a) indicate that no counts were observed for that diameter particle at that time. Panel (c) shows the observed (black) and predicted (red) CCN concentrations averaged over the Aug. 10-15, 2011 time period. The blue circles are the simulations when nucleation is not included, which demonstrates the importance of particle nucleation for CCN formation.